AD-A040 988 JOHNS HOPKINS UNIV LAUREL MD APPLIED PHYSICS LAB F/G 4/1
STATISTICAL MODELS OF SUMMER RAIN SHOWERS DERIVED FROM FINE-SCA--ETC(U)
APR 77 T G KONRAD N00017-72-C-4401
UNCLASSIFIED APL/JHU-CP-056 NL

1 OF 1
AD A040988

END
DATE FILMED
7-77

APL/JHU
CP 056
APRIL 1977

AD A040988

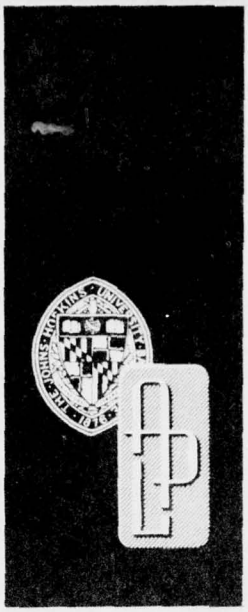

Meteorology

STATISTICAL MODELS OF SUMMER RAIN SHOWERS DERIVED FROM FINE-SCALE RADAR OBSERVATIONS

by T. G. KONRAD

DDC
RECEIVED
JUN 28 1977
A

THE JOHNS HOPKINS UNIVERSITY ▪ APPLIED PHYSICS LABORATORY

DISTRIBUTION STATEMENT A
Approved for public release;
Distribution Unlimited

AD No.
DDC FILE COPY

BIBLIOGRAPHIC DATA SHEET	1. Report No. APL/JHU-CP 056	2.	3. Recipient's Accession No.
4. Title and Subtitle Statistical Models of Summer Rain Showers Derived from Fine-Scale Radar Observations			5. Report Date April 1977 6.
7. Author(s) Thomas G. Konrad			8. Performing Organization Rept. No. CP 056
9. Performing Organization Name and Address The Johns Hopkins University Applied Physics Laboratory Johns Hopkins Rd. Laurel, MD 20810			10. Project/Task/Work Unit No. Task W01 11. Contract/Grant No. N00017-72-C-4401
12. Sponsoring Organization Name and Address National Aeronautics and Space Administration Code 953 Goddard Space Flight Center Greenbelt, MD 20771			13. Type of Report & Period Covered Civil Programs 14.

15. Supplementary Notes

16. Abstracts

The fine-scale, three-dimensional structure of summer rain showers in the mid-Atlantic region has been analyzed using data from a high-power, narrowbeam radar coupled with automatic data sampling and recording equipment. Statistical descriptions of the rain cells in terms of a variety of physical cell parameters such as core reflectivity, contour area, and altitude extent have been generated along with the frequency of occurrence for various storm classes and categories. The statistical descriptions of the rain cells were compared with those from previous investigators at other geographical locations. Simplified models of rain cells based on the statistical descriptions are developed for different rain categories as a function of frequency of occurrence.

17. Key Words and Document Analysis. 17a. Descriptors

rainfall
radar echoes
meteorological radar
statistical analysis

17b. Identifiers/Open-Ended Terms

rain structure
models

17c. COSATI Field/Group 04/02

18. Availability Statement	19. Security Class (This Report) UNCLASSIFIED	21. No. of Pages 67
	20. Security Class (This Page) UNCLASSIFIED	22. Price

FORM NTIS-35 (REV. 3-72) THIS FORM MAY BE REPRODUCED USCOMM-DC 14952-P72

APL/JHU
CP 056
APRIL 1977

Meteorology

STATISTICAL MODELS OF SUMMER RAIN SHOWERS DERIVED FROM FINE-SCALE RADAR OBSERVATIONS

by T. G. KONRAD

DDC
RECEIVED
JUN 28 1977
A

THE JOHNS HOPKINS UNIVERSITY ■ APPLIED PHYSICS LABORATORY
Johns Hopkins Road, Laurel, Maryland 20810

DISTRIBUTION STATEMENT A
Approved for public release;
Distribution Unlimited

THE JOHNS HOPKINS UNIVERSITY
APPLIED PHYSICS LABORATORY
LAUREL MARYLAND

ABSTRACT

The fine-scale, three-dimensional structure of summer rain showers in the mid-Atlantic region has been analyzed using data from a high-power narrowbeam radar coupled with automatic data sampling and recording equipment. Statistical descriptions of the rain cells in terms of a variety of physical cell parameters such as core reflectivity, contour area, and altitude extent have been generated along with the frequency of occurrence for various storm classes and categories. Rain cell classes and categories were based on the reflectivity levels at essentially ground level. Cell populations that include all the cells observed were also treated. The mean and median core reflectivity profiles are essentially constant up to altitudes of 4 to 6 km and then fall off with increasing altitude and follow an orderly progression with cell category. The area of the reflectivity contours about the core value was found to follow an exponential relationship.

The statistical descriptions of the rain cells for the mid-Atlantic region were compared with those from previous investigators at other geographical locations. In terms of core reflectivity profiles, the data for the various locations are similar. However, significant differences are evident in the altitude extent. Finally, simplified models of rain cells based on the statistical descriptions were developed for the different rain categories as a function of frequency of occurrence.

ACCESSION for
NTIS White Section
DDC Buff Section
UNANNOUNCED
JUSTIFICATION
BY
DISTRIBUTION/AVAILABILITY CODES
Dist. AVAIL. and/or SPECIAL
A

CONTENTS

PRECEDING PAGE BLANK-NOT FILMED

ILLUSTRATIONS

1. INTRODUCTION

The most serious problems in the design of terrestrial and earth-satellite microwave communication systems are the attenuation of the signal due to rain along the path and the interference due to scattering by the precipitation particles. Crane (Ref. 1) and, more recently, Hogg and Chu (Ref. 2) have reviewed these effects in some detail along with other sources of signal degradation. The difficulties become especially severe at the very high frequencies being considered and implemented for communication purposes, i.e., in the tens of gigahertz frequency range. The physics of the attenuation and scattering processes are fairly well understood, but the communication design engineer requires a statistical description, or model, of the spatial and temporal characteristics of precipitation elements to make predictions of overall systems performance that include estimates of expected attenuation and interference effects and the advantages of path diversity techniques.

At the request of the Office of Telecommunications, the National Aeronautics and Space Administration (NASA) planned and implemented a broad program directed toward the measurement and characterization of propagation and interference effects in space communication applications. The various elements of this program are discussed by Eckerman (Ref. 3). One facet of the program was concerned with the statistical modeling of rainstorm characteristics based on high-resolution radar measurements of the rain intensity and structure.

The objectives of the experiment were: (a) to determine the detailed structure of individual cells, leading to a statistical description or model of an individual rain cell in terms that

---

Ref. 1. R. K. Crane, "Propagation Phenomena Affecting Satellite Communication Systems Operating in the Centimeter and Millimeter Wavelength Bands," Proc. IEEE, Vol. 59, No. 2, 1971, pp. 173-188.

Ref. 2. D. C. Hogg and T. Chu, "The Role of Rain in Satellite Communications," Proc. IEEE, Vol. 63, No. 9, 1975, pp. 1308-1331.

Ref. 3. J. Eckerman, "A NASA Program to Characterize Propagation and Interference for Space Applications," AIAA 4th Communications Satellite Systems Conference, 1972, No. 72-577, AIAA, New York.

PRECEDING PAGE BLANK-NOT FILMED

would be useful to both communications engineers and meteorologists, and (b) to determine statistics of the field of rain cells such as number density and cell spacing. Complete details of the program are contained in a three-volume final report (Refs. 4 to 6). This paper summarizes the major elements of the experimental and analytical portions of the program and presents statistical descriptions for a variety of rain cell parameters. In addition, a comparison of the results with previous investigations and a modeling procedure using the statistical descriptions are included.

Ref. 4. I. Katz, A. Arnold, J. Goldhirsh, T. G. Konrad, W. L. Vann, E. B. Dobson, and J. R. Rowland, "Radar Derived Spatial Statistics of Summer Rain — Experiment Description," Vol. I, Final Contractors Report, NASA CR-2592, 1975.

Ref. 5. T. G. Konrad and R. A. Kropfli, "Radar Derived Spatial Statistics of Summer Rain — Data Reduction and Analysis," Vol. II, Final Contractors Report, NASA CR-2592, 1975.

Ref. 6. "Radar Derived Spatial Statistics of Summer Rain — Appendices," Vol. III, Final Contractors Report, NASA CR-2592, 1975.

2. EXPERIMENTAL DESCRIPTION

The experiment was performed at the NASA/Wallops Flight Center, Wallops Island, Virginia, during May through August 1973, using the high-resolution Space Range Radar (SPANDAR). Wallops is located on the mid-Atlantic coast just south of the Maryland-Virginia line.

The SPANDAR radar, a high-power, narrowbeam radar operating at S band (10.7-cm wavelength), was originally designed for long-range tracking. The system is highly versatile, with variable transmitted power, polarization, pulse length, and pulse repetition rate. During this experiment, the peak power transmitted was 1.0 MW at a pulse length of 1.0 μs and a PRF of 960. The antenna is a 60-ft parabolic dish with a beamwidth of 0.36° in the vertical and 0.44° in the horizontal. The radar was operated with vertical polarization.

Changes and additions occasioned by the specific needs of the experiment were made in the original radar configuration. Generally, the changes were in the interest of measurement resolution and accuracy, and included frequency diversity, computer control of the antenna mount, and extended linear range of the receiver.

It is well known that radar returns from meteorological targets fluctuate from pulse to pulse; therefore it is necessary to average a number of statistically independent pulses to measure radar reflectivity reliably. A more detailed discussion of this point is contained in a subsequent section on measurement accuracy. The greatest number of pulses averaged is generally limited by scanning considerations, while the shortest meaningful time between pulses to be averaged depends on their time-to-independence. For typical weather targets at S band, the time-to-independence is about 10 to 30 ms as shown by Atlas (Ref. 7) and Marshall and Hitschfeld (Ref. 8). Frequency diversity is a practical method for achieving independent samples quickly. Wallace (Ref. 9) shows that

---

Ref. 7. D. Atlas, "Advances in Radar Meteorology," Adv. Geophys., Vol. 10, Academic Press, New York, 1964, pp. 318-478.

Ref. 8. J. S. Marshall and W. Hitschfeld, "Interpretation of the Fluctuating Echo from Randomly Distributed Scatterers: Part I," Can. J. Phys., Vol. 31, 1953, pp. 962-994.

Ref. 9. P. R. Wallace, "Interpretation of the Fluctuating Echo from Randomly Distributed Scatterers: Part II," Can. J. Phys., Vol. 31, 1953, pp. 995-1009.

independence can be achieved by shifting the transmitted frequency from pulse to pulse by an amount given by τ^{-1}, where τ is the pulse length. With a 1-μs pulse and a 1-kHz PRF, for example, the frequency must be shifted by at least 1 MHz for about 20 successive pulses before it is returned to its original value. The frequency diversity technique implemented for this program consisted of an interlace mode where the frequency interval between successive frequency steps was 12 to 13 MHz; that is, the frequency was stepped up 13 MHz and down 12 MHz. This interlace pattern was selected to minimize second- (or even third-) time-around problems. Such interference can be a problem of high-power, sensitive radars in the presence of distant heavy rain. For a frequency shift of 12 to 13 MHz, the second-time-around returns fall well outside the receiver bandwidth while the 1-MHz separation between every other pulse is maintained.

The linear dynamic range of the receiver was extended to accommodate both the weak returns at long range and the strong returns at close range. The criteria used to select the required receiver dynamic range were a rain rate of 1 mm/h at a range of 140 km for the weakest return and a 75-dBZ reflectivity factor return at a range of 10 km for the strongest return. Assuming an additional 10-dB pulse-to-pulse fluctuation in the signal, these criteria resulted in a 90-dB linear range requirement. A new solid-state log IF amplifier was designed and added to the radar system to extend its linearity over this range.

In contrast with most of the previous research performed with the Wallops radars where manual operation of the antenna mount was adequate, this experiment required antenna raster scan sequences to be executed with little loss of time between individual antenna sweeps, i.e., before any appreciable change could take place in the reflectivity structure of the rain cell. A PDP-8 computer was interfaced with the antenna mount to perform both range height indicator (RHI) and plan position indicator (PPI) scan sequences rapidly and automatically. With this new capability, stored programs for various scan sequences could be called up quickly via teletype control. Complete three-dimensional snapshots of cell structures were scanned within roughly a 4-min interval; this included azimuthal sectors up to 360° and vertical sectors up to 75° elevation. Of course, the time required to scan a rain cell depends on the antenna sweep rate. This is discussed in a subsequent section on measurement resolution and accuracy.

The data acquisition system designed for this experiment consisted of the on-line signal processing and digital recording system and the off-line video recording system. In the on-line system,

the returned signal was sampled in each of 871 range bins or range resolution cells, digitized, integrated, and recorded. The integrator is capable of averaging from 64 to 1024 pulses in each resolution cell. The output of the integrator was recorded on a nine-channel, 1600-bits/in. synchronous tape recorder operating at 45 in./s. Antenna position, time, signal processing parameters, and other pertinent radar parameters including pulse-to-pulse calibration signals were recorded on the digital tape, in addition to the integrated output from each resolution cell. Control of the signal processing and digital recording systems was also provided by the PDP-8 computer.

The overriding consideration in the selection of the radar operating conditions and the signal processing and recording equipment for the experiment was the preservation and exploitation of the high spatial resolution available with the SPANDAR radar. The resolution in range was matched to the pulse length of 1 μs, while the resolution in azimuth was chosen as one beamwidth. Given a desired azimuthal resolution, the selection of the sweep rate, PRF, and pulses to be integrated is a compromise between accuracy of measurement and time required to scan the rain cell. For a stationary process, one obtains a more accurate measure of reflectivity as the number of pulses increases. The use of more than roughly 100 samples, however, improves accuracy only very slowly. A very high PRF places severe demands on the signal processing equipment, while slow scanning increases the probability that the cell structure will change during the raster scan. The operating conditions selected were a sweep rate of 3°/s, with 128 pulses being integrated at a PRF of 960/s. This results in one integrated sample each beamwidth with roughly 4 min needed to scan a rain cell with a series of PPI sweeps for every kilometer in altitude.

An extensive calibration program was performed both prior to and during the experiment. The pre-experiment program was concerned primarily with the measurement of system characteristics such as antenna pattern, antenna gain, transmitter bandwidth, transmitted power, transmitter and receiver line losses, receiver noise figure, and bandwidth. The stability of the system was checked over the short term (minutes and hours) and the long term (months). Corrections of the measured power were included to account for the underestimation of average power received because of integration of the logarithm of power (Ref. 8) and quantization of the signal at both the input and output of the signal processor (Austin and Shaffner, Ref. 10). The overall uncertainty of the radar calibration and stability was determined to be within ±2 dB.

Ref. 10. J. M. Austin and M. R. Shaffner, "Computations and Experiments Relative to Digital Processing of Weather Radar Echoes," Preprints 14th Radar Meteorology Conference, American Meteorological Society, Boston, 1970, pp. 375-380.

The second aspect of the calibration program concerned the monitoring and/or logging of critical points in the radar system during the experiment. Certain parameters such as transmitted power were recorded continuously. Calibration signals and receiver noise samples were recorded on the digital tape on a pulse-to-pulse basis. They were used to show changes that occurred in the radar system characteristics or calibration during data taking.

Two modes of operation corresponding to the two experiment objectives discussed above were used during the experiment. The first was to determine the characteristics of the field of rain cells. A complete PPI sweep was made at an elevation angle of 2° at half-hour intervals. This interval was chosen so that the rain cells used in the subsequent statistical analysis would be (essentially) independent. Several investigators had shown that the typical lifetime, or duration, of a rain cell is about 30 min, e.g., Austin (Ref. 11), Chisholm (Ref. 12), and Battan (Ref. 13).

The second mode of operation was to record the detailed reflectivity structure of individual rain cells. A PPI raster scan was made over a selected sector, generally 60° in azimuth. The scan was started at an elevation of 0.5°, and the increments in elevation angle were chosen to correspond to altitude spacing of roughly 1 km or less throughout the height of the precipitation structure. The scans occasionally were repeated rapidly to record the changes in cell structure with time.

In order to maximize the chances of observing precipitation activity, the radar observations were made from 3 to 11:30 p.m. EST.

During the four-month period, rain showers within a 75-nmi radius were observed on 33 days. A total of 403 PPI raster scans was recorded with an average of 10 sweeps per scan through the rain cell structures.

Ref. 11. P. M. Austin, "Application of Radar to Measurement of Surface Precipitation," Technical Report ECOM 01472-3, Semi-Annual Report 3, Contract DA 28-043 AMC-01472(E), Massachusetts Institute of Technology, 1967.

Ref. 12. A. J. Chisholm, "Small Scale Radar Structure of Alberta Hailstorms," Preprints 12th Radar Meteorology Conference, American Meteorological Society, Boston, 1966, pp. 339-341.

Ref. 13. L. J. Battan, "Duration of Convective Radar Cloud Units," Bull. Am. Meteorol. Soc., Vol. 34, 1953, pp. 227-228.

3. DATA REDUCTION AND PROCESSING

The primary data for the reduction and analysis phases of the program were the computer-compatible digital magnetic tapes containing the integrated log power received in each of 871 range gates made during PPI raster scans through the field of rain cells. The first step in the reduction process was to identify the peaks or local maxima in power received from each PPI sweep in a scan. All the data for a given sweep were read into core memory of an IBM 360/95 computer as a two-dimensional array. The computer then performed a search routine in this array to find the maxima of log power received. Although all the data for a sweep were read into core, only areas that contained rain cells were searched. Thus, areas that contained no rain and areas of known ground clutter were eliminated.

The peak reflectivity* factor was then computed using the integrated power received, the range, and the standard radar equation for meteorological targets. Since no in situ information was available concerning the state of the precipitation, the reflectivity factor was calculated assuming that all the returns were from rain. Thus, the reflectivity referred to herein is actually the equivalent radar reflectivity factor.

Having identified the peak locations, the computer then calculated the altitude of the peak, the contours of constant reflectivity about each peak using a compare-and-minimize algorithm, the contour area, the length and width of the contour through the centroid of the area, the orientation of the major axis of the contour, and all interpeak distances.

The next step was to identify in each PPI raster scan the peaks that made up a rain cell. The computer assigned a number to each peak in a sweep as it was found. The peak numbers associated with a given rain cell at the various PPI sweeps (or altitudes) are not necessarily the same from sweep to sweep due, for example, to spurious local maxima. The following manual procedure was used to identify the peaks in each sweep of a scan that made up the same cell. The location, range, and azimuth of all peaks found in all

*In many of the reports dealing with radar descriptions of rain showers discussed in a following section, the peak reflectivity is also referred to as the core reflectivity. The two terms will be used interchangeably herein.

sweeps of a scan were plotted (Fig. 1 is an example). The cells were identified based on the fact that peaks associated with the same rain cell are clustered. A rain cell was defined as an identifiable cluster of peaks with consecutive sweep numbers, e.g., cell B in Fig. 1. All cell identification was performed by one individual so that the same criteria were used, subjective though they may be.

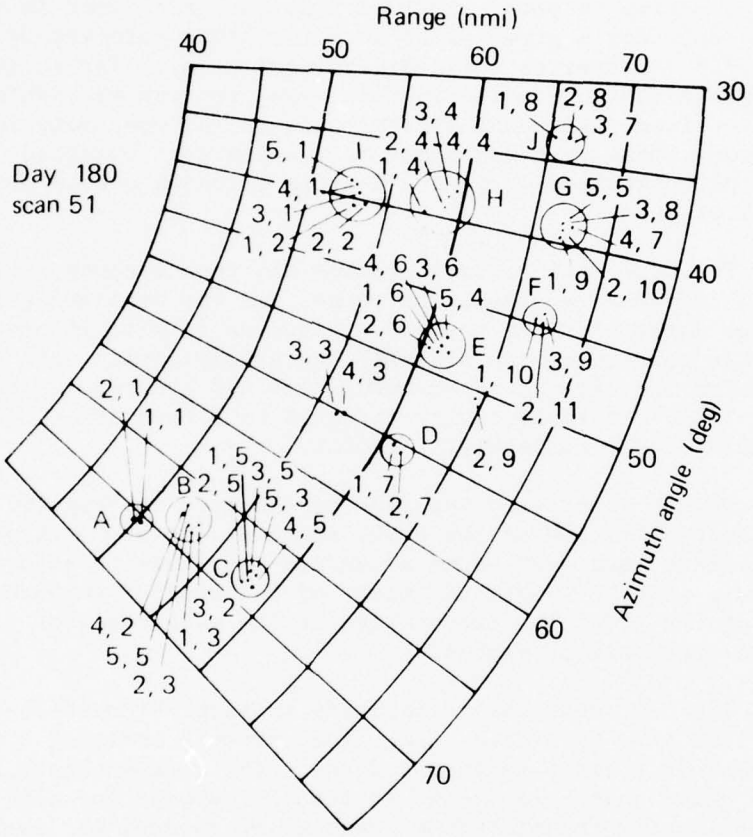

Fig. 1 Peak Locations for Complete Scan. The first number in a pair is the sweep number, the second is the peak number (e.g., 2, 3 indicates sweep 2, peak 3). The circles enclose a cluster of peak locations; size does not indicate cell size. The letters are rain cell identification.

In order to ensure that the cells used in the statistical analysis were (essentially) independent, only the raster scans separated by one half hour were used, as discussed above. This eliminated scans that were taken very rapidly for time history and cell development analysis. The assumption was that, although the rain cell itself may be the same for scans separated by one half hour, its characteristics have changed sufficiently so that the observations may be considered to be independent.

With the above restriction on the data, 185 PPI scans through rain cells on 21 days during the four-month observation period were included in the statistical analysis of individual cell characteristics. The 1141 identifiable cells were further classified and categorized as follows. Cells whose core reflectivity at the lowest elevation angle was greater than 30 dBZ were classified as rain-on-the-ground (ROG) cells. The altitude at a range of 70 nmi at the starting elevation angle of 0.5° is 2 km. Cells at a closer range, of course, are observed at lower altitudes. Cells whose reflectivity was less than 30 dBZ at altitudes below 2 km were classified as "virga." The term virga, not used in its strict meteorological sense of no rain reaching the ground, simply indicates a class of cell with very low reflectivity and rain rate at ground level. The reflectivity threshold of 30 dBZ was chosen to restrict the analysis to cells with high core reflectivities that represent a potential problem for communications from the standpoint of attenuation and interference caused by scattering. This paper is concerned with the statistical modeling of the ROG class of cell only, except where noted. Statistical descriptions of the virga class of cell similar to those presented below were also compiled and are contained in the program's final report (Ref. 5) but are not presented here.

The cells in the ROG class were further subdivided into seven categories according to their reflectivity value at the lowest elevation angle, each category being 5 dBZ wide starting at 30 dBZ. Categorizing the cells in this manner allows a comparison with ground-based measurements of rainfall rate from rain gauges and provides a means for extrapolating the data from this experiment to other locations based on the frequency of occurrence of various rain intensities at ground level.

When the cells were identified and classified, two profile shape parameters were computed for each cell: the reflectivity ratio, which is the ratio of the maximum core reflectivity in a cell to that at the lowest elevation angle, and the altitude of the maximum reflectivity. These parameters are similar to those

examined by Donaldson (Ref. 14) and Inman and Arnold (Ref. 15). If the maximum core reflectivity occurred at the lowest elevation angle, the reflectivity ratio is 1.

Ref. 14. R. J. Donaldson, "Radar Reflectivity Profiles in Thunderstorms," J. Appl. Meteorol., Vol. 18, 1961, pp. 292-305.

Ref. 15. R. L. Inman and J. E. Arnold, "Thunderstorm Characteristics. Final Report," Texas A&M University, Contract AF 19(604)-6136, 1961, pp. 8-73.

4. STATISTICAL DESCRIPTIONS

Frequency distributions of the core reflectivities, areas of the contours 6 and 10 dBZ down from the peak, the contour length-to-width ratio, and the orientation of the contour major axis were determined for each category of cell as a function of altitude. The arithmetic mean, median, and standard deviation for all these distributions were also calculated. Profiles of reflectivity were constructed using the mean and median values. Distributions of the number of cells in each category for each 1-km altitude interval were compiled. Conversely, the number of cells at each altitude for a given category were computed. These distributions can be used to show the height to which cells of different intensities are expected to extend, as will be discussed later.

Since there is a large number of distributions for all the combinations of parameters, categories, and altitude intervals, only representative samples are presented here. The complete set of data with all distributions and profiles is contained in the final report on the program (Ref. 5). Although not strictly correct mathematically, the cumulative frequency distributions are referred to and interpreted in the following discussion as conditional probabilities.

CORE REFLECTIVITY

In compiling the frequency distributions of core reflectivities at each altitude for each category of rain cell, only cells that reached that altitude were included in the population. That is, no zeros were included when a cell failed to extend to some altitude interval. The absolute frequency of occurrence of any core reflectivity value must include both the probability that a cell reaches a given altitude and the probability that it has that core reflectivity.

An example of the frequency distributions of core reflectivities for the population of cells in the 55- to 60-dBZ category is shown in Fig. 2. Similar distributions were compiled for all the rain categories. Note the rather orderly progression of the distributions with increasing altitude. The curves may be interpreted as follows. If a rain cell with a core reflectivity between 55 and 60 dBZ at the ground reaches some altitude, what is the

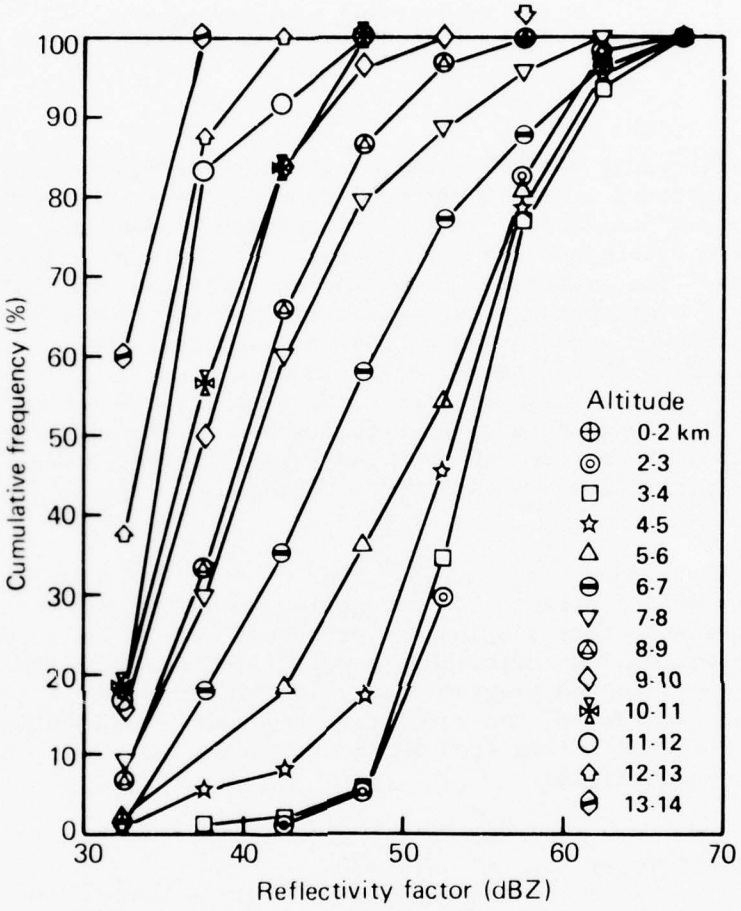

Fig. 2 Cumulative Frequency Distributions of Core Reflectivity Factor according to Altitude for Cells in 55- to 60-dBZ Category; 87 Cases

probability that the core reflectivity at that altitude will be equal to or less than some value? The probability of a core reflectivity at 0 to 2 km being equal to the category value (e.g., 55 to 60 dBZ) is 100%, of course, since the population of rain cells used to construct these distributions contains only cells with a reflectivity in this range at the ground level.

Frequency distributions like those in Fig. 2 may also be used to answer other questions. For example, given that it is raining

on the ground with some intensity (reflectivity below 2 km of some value), what is the maximum value of reflectivity experienced as a function of altitude? This is simply the cross plot of the core reflectivity values at a frequency of 100% for each category of cell. Alternatively, given the rain intensity (reflectivity) at ground level, what is the probability that this value is exceeded at each altitude? Again, this is a cross plot of data similar to those in Fig. 2 for each category. The probability that the surface value is exceeded is 100 minus the probability of frequency of occurrence at each altitude for a reflectivity equal to that on the ground, i.e., the category value. For example, in Fig. 2, given a surface reflectivity of 55 to 60 dBZ, the probability that the reflectivity at 6 to 7 km is greater than 55 to 60 dBZ is 13% (100 minus the value at 57.5 dBZ for 6 to 7 km; 100 - 87 = 13).

The mean and median core reflectivity factors for each category and altitude interval were calculated using the original core reflectivity data. Profiles of mean and median core reflectivity for the seven categories are shown in Figs. 3 and 4, respectively. Included in the figures is the number of cells in each category that were included in the profiles. For the higher reflectivity categories, the number of cells is rather small, indicating a lower level of statistical confidence in both the frequency distribution and the mean and median values. With the exception of the 65- to 70-dBZ category, the profiles do not exhibit any appreciable "knee" at altitude. This is consistent with Donaldson (Ref. 14) and Inman and Arnold (Ref. 15), among others, for rain showers. There is an orderly progression of the curves with category, and the tendency for the more intense rain cells to reach higher altitudes is clearly evident. This point is discussed further below.

For some applications, the breakdown of the rain cell population into categories may be too detailed, and a grosser representation of the rain cell structure is sufficient. Distributions and core profiles of reflectivity were also compiled using all the ROG class cells identified during the entire four-month observation period regardless of category, i.e., the entire population. In this case, the only condition is that the rain cell must have a reflectivity greater than 30 dBZ in the lowest altitude interval, as was described earlier. Figure 5 shows the cumulative frequency distributions using all the cells. Note that for clarity only every other altitude interval is shown.

The mean and median core reflectivity profiles using all the cells are presented in Fig. 6. The effect of the 30-dBZ threshold is evident in these curves. Since no core reflectivities below 30 dBZ were included, the frequency of occurrence in Fig. 5 is somewhat

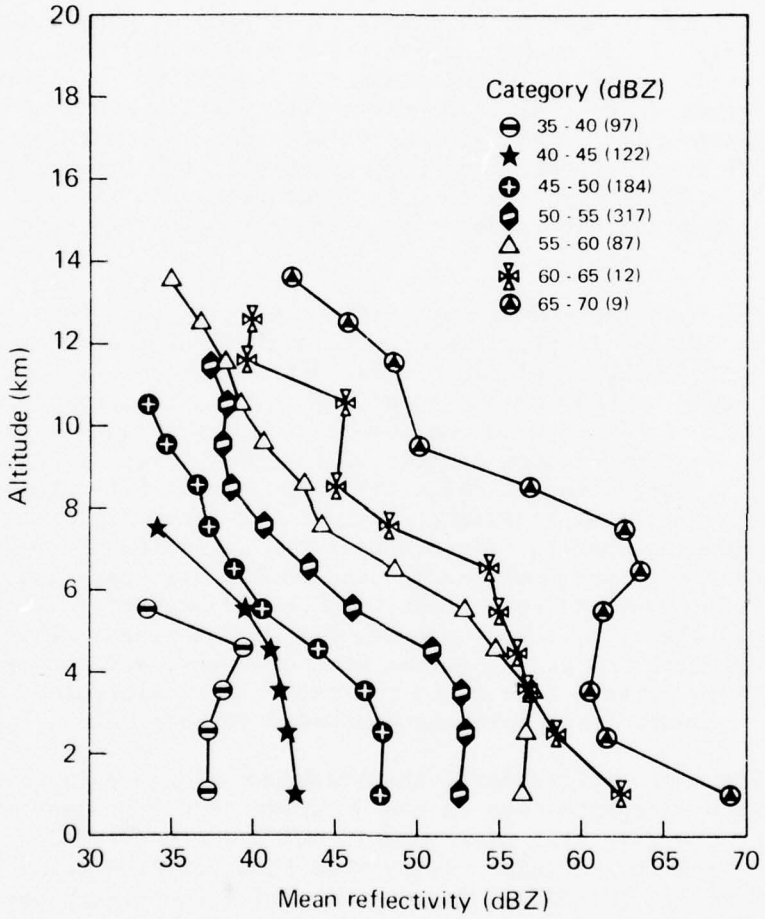

Fig. 3 Profiles of Mean Core Reflectivity for Various Categories of Rain Showers. The number of cells in each category is shown in parentheses.

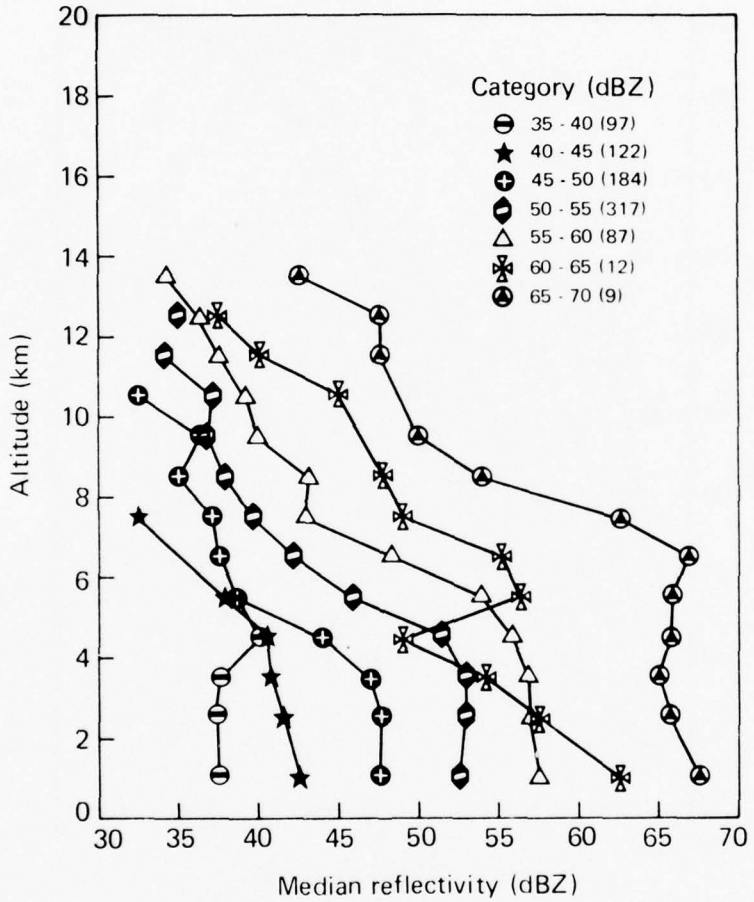

Fig. 4 ***Profiles of Median Core*** **Reflectivity for Various Categories of Rain Showers. The number of cells in each category is shown in parentheses.**

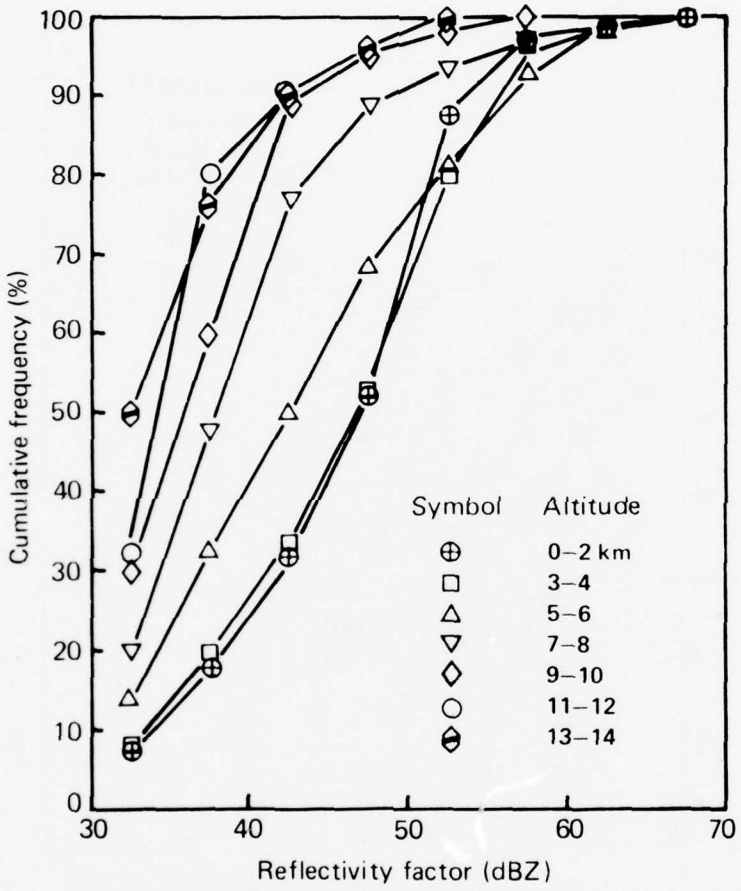

Fig. 5 Frequency Distributions of Core Reflectivity Factor According to Altitude for All Cells Observed Regardless of Category

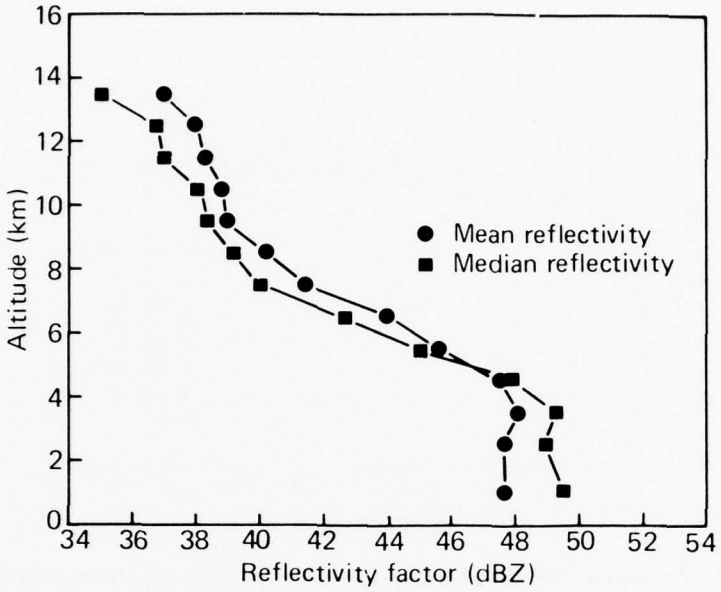

Fig. 6 Profiles of Mean and Median Core Reflectivity for All Cells Observed

high for distributions in which the tail of the reflectivity distribution at the lower values is truncated significantly by the 30-dBZ threshold. The distributions at altitude intervals of 9 to 10 km and above are certainly affected as they are, to a lesser extent, at 7 to 8 km. In turn, the mean and median values in Fig. 6 are too large. A more pronounced falloff of core reflectivity with altitude should be expected at altitudes above roughly 8 km.

REFLECTIVITY RATIO AND HEIGHT OF MAXIMUM REFLECTIVITY

The reflectivity ratio distributions for the various categories of rain cells are shown in Fig. 7; the distribution considering all cells is shown in Fig. 8. No interpolation or curve fitting of the individual cell core reflectivity profiles was performed by the computer in establishing the maximum reflectivity value for each cell. The procedure was simply to save the largest value of core reflectivity found during the PPI raster scan through a given cell. The maximum core reflectivity thus obtained is somewhat less than the actual maximum unless the PPI sweep intercepts

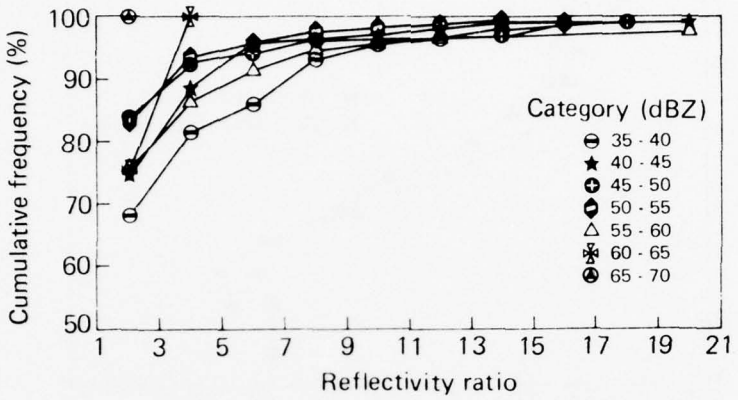

Fig. 7 Frequency Distributions of Reflectivity Ratio for Various Cell Categories

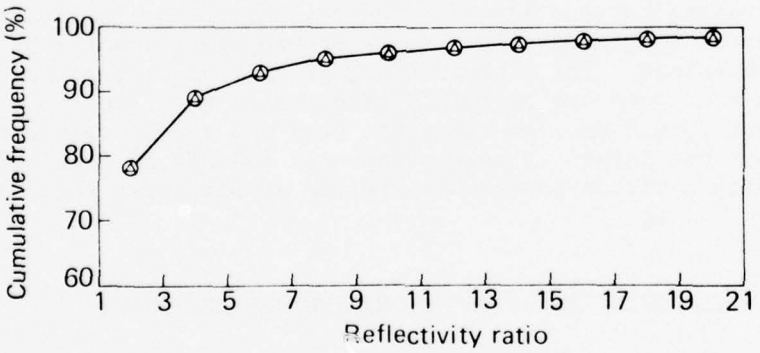

Fig. 8 Frequency Distribution of Reflectivity Ratio for All Cells Regardless of Category

the cell exactly at the real maximum value, a fairly unlikely coincidence. Therefore, the distributions shown are somewhat high; i.e., the percent probability that a reflectivity ratio is equal to or less than some value will be slightly lower. The distributions indicate that in the vast majority of cases the maximum core reflectivity or rain rate is located at or just above ground level. In Fig. 8, for example, 78% of the cases fell in the first reflectivity ratio interval of 1 to 3.

The distributions of the altitude of the maximum core reflectivity (when it did occur) are shown in Figs. 9 and 10. In Fig. 10, the median height is 2 km, and roughly 90% of the cases

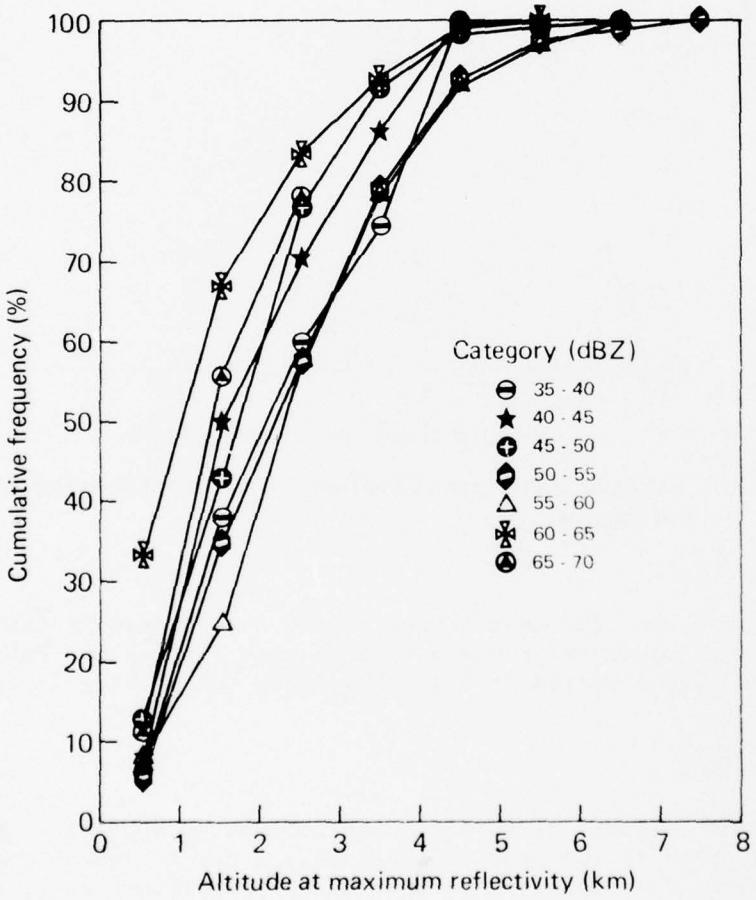

Fig. 9 Distributions of Altitude of Maximum Core Reflectivity for Various Cell Categories

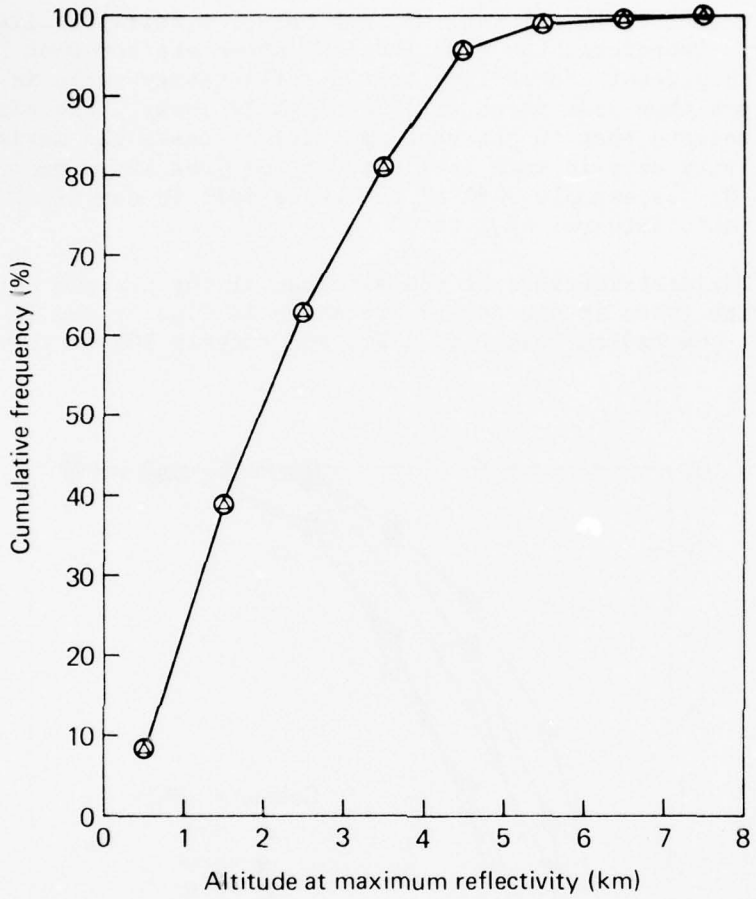

Fig. 10 Altitude of Maximum Core Reflectivity for All Cells Regardless of Category

are below 4 km. The mean height of the zero degree isotherm for the days of observation was 4.8 km so that the maximum reflectivity generally occurred considerably below the melting layer.

CONTOUR AREA

The contours of reflectivity calculated about each peak were relative to the peak reflectivity, i.e., a constant number of dBZ down from the core value. Relative contours at 3, 6, and 10 dBZ down were generated, and the contour area was determined along with the maximum and minimum dimensions through the area

centroid and the orientation of the major axis of the contour. Considerable difficulty was experienced in the generation of the 3 dB down contours; therefore only the 6 and 10 dB down contours were used in the analysis.

Hudlow and Scherer (Ref. 16) found that an exponential relationship existed between the received power at a given gain threshold and the square root of the echo area persisting at that threshold for a given maximum return from the cell center. The present data were examined to see if the exponential square root of area relationship was applicable in the case of reflectivity using the 6 and 10 dB down contours along with the local peak reflectivity. Plots of reflectivity in dBZ versus the square root of contour area for 125 cells at various altitudes indicate that the exponential function is a reasonable model of the contour area distribution about a cell core. Thus, we may write

$$Z_c = Z_p \, 10^{b\sqrt{A_c}} \tag{1}$$

or

$$Z_p(\text{dBZ}) - Z_c(\text{dBZ}) = - b\sqrt{A_c} \tag{2}$$

where Z_p is the core reflectivity at a given altitude, Z_c is some contour value about Z_p, b is the slope, and A_c is the area of contour Z_c. The model is shown schematically in Fig. 11. The slopes of the area-versus-reflectivity curves were collected according to the core reflectivity of the echo in 5-dBZ increments to see if there was any dependence on cell intensity. Figure 12 shows the average slope for each core reflectivity interval. There is a definite trend with the higher slopes that is associated with the weaker cells, i.e., lower peak reflectivity. The total variation in the average slope is about a factor of two from the weakest to the most intense cell.

If we ignore the variation of the slope with core reflectivity and include all the cells in a single population, the probability distribution is highly skewed and concentrated at the low slope values, as is shown in Fig. 13. This fact is useful in the cell modeling procedure discussed in a subsequent section.

Ref. 16. M. D. Hudlow and W. D. Scherer, "Precipitation Analysis for BOMEX Period III," NOAA Technical Report EDS 13, 1975.

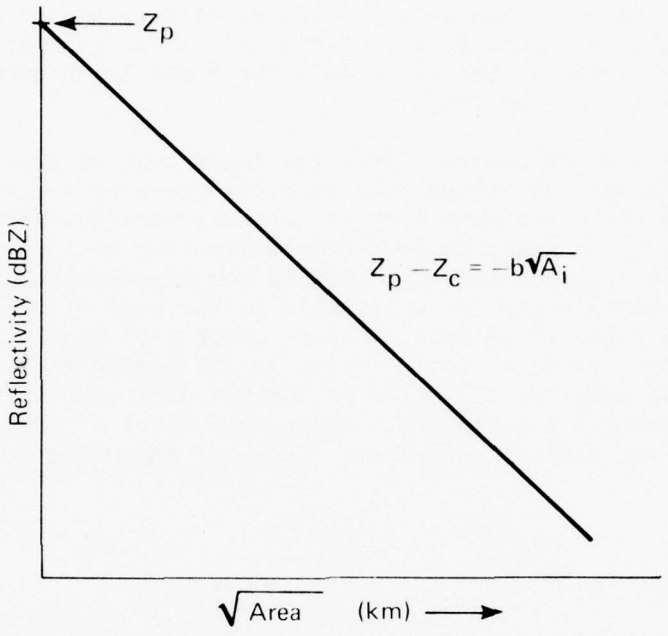

Fig. 11 Schematic of Exponential Contour Area Representation (see text for symbols)

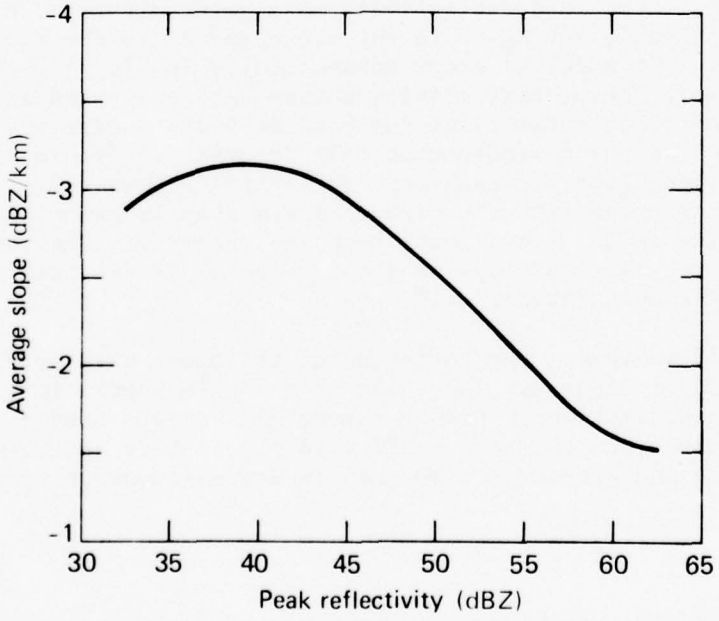

Fig. 12 Average Slope for Each Core Reflectivity Interval

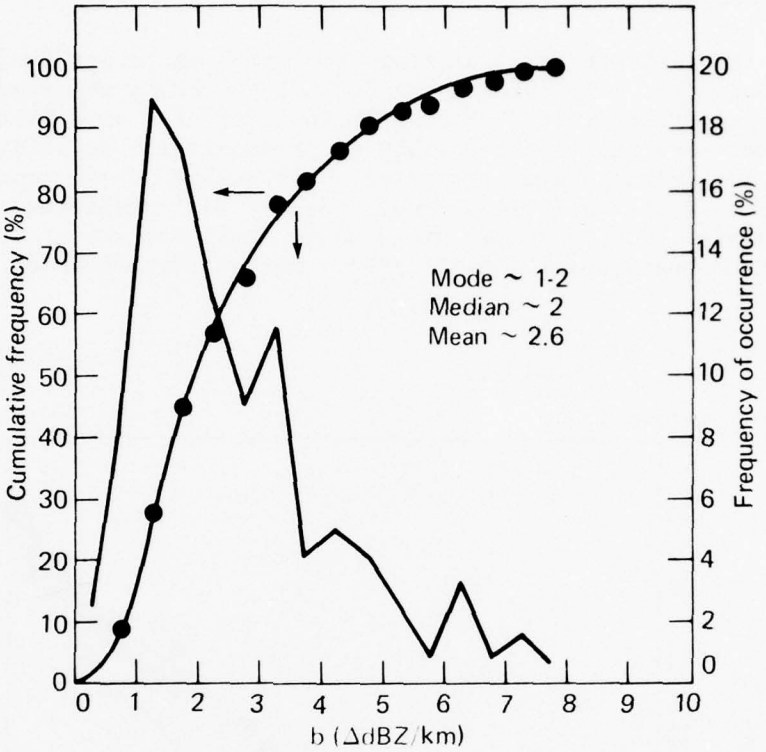

Fig. 13 Distribution of Slopes Using All Cells in a Single Population

LENGTH-TO-WIDTH RATIO

In general, the cumulative distributions show that 50% of the cells have a length-to-width ratio of three or less regardless of reflectivity interval, category, or altitude. Roughly 80% have ratios of six or less. However, no consistent identifiable variation in the length-to-width ratio was found with any of the sorting parameters. There is some indication that the cells at lower altitudes have higher ratios than the cells at altitude. Such conclusions must be tempered by the fact that there are fewer cells at altitude and the statistical confidence is low. It should also be remembered that the calculated length-to-width ratio is not the result of fitting by an ellipse or any other shape. It is simply the ratio of the maximum dimension through the centroid of the 10-dB contour area to the minimum dimension. It is intended only as a rough indicator of contour shape.

CONTOUR ORIENTATION

Figure 14 presents an example of the cumulative frequency distribution of cell orientation for all the cells observed in the local peak reflectivity interval of 40 to 45 dBZ, as a function of altitude. The distributions show no identifiable variation with any of the sorting parameters used. All angles appear equally probable. Where deviations occur, such as for an altitude of 8 to 9 km in Fig. 10, the number of cases is small and the distribution has little statistical significance. Further breakdown of the cell

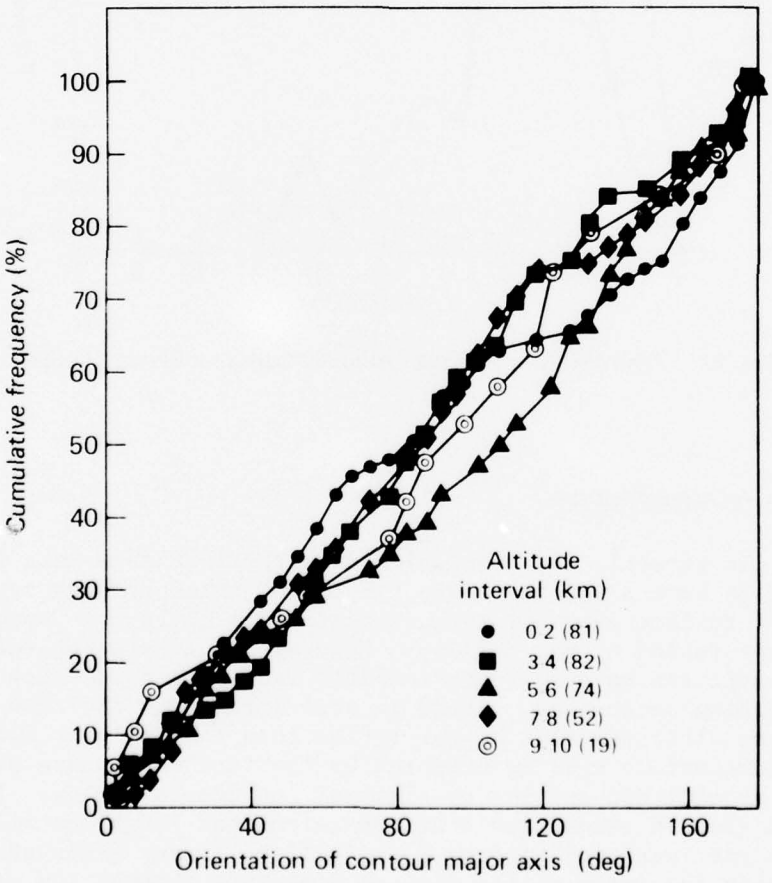

Fig. 14 Frequency Distributions of Orientation of 10-dB-Down Contour Major Axis for Cells Having Core Reflectivities in 40- to 45-dBZ Interval at Various Altitudes

population into cells associated with frontal activity may show some preferred orientation, e.g., along the front or with the wind direction. The data presented here contain no such breakdown, and the results apply to all the cells observed during the four-month period.

FREQUENCY OF OCCURRENCE OF RAIN CATEGORIES

As noted above, the distributions of the number of cells were compiled according to category for a given altitude interval and at each altitude for a given category. Of particular interest is the distribution of cell reflectivities in the lowest altitude interval since this distribution may be compared with ground-based rainfall rate data from other locations for extrapolation purposes. Figure 15 shows the frequency of occurrence and cumulative frequency of rain intensity (cell category) at the ground using all the cells

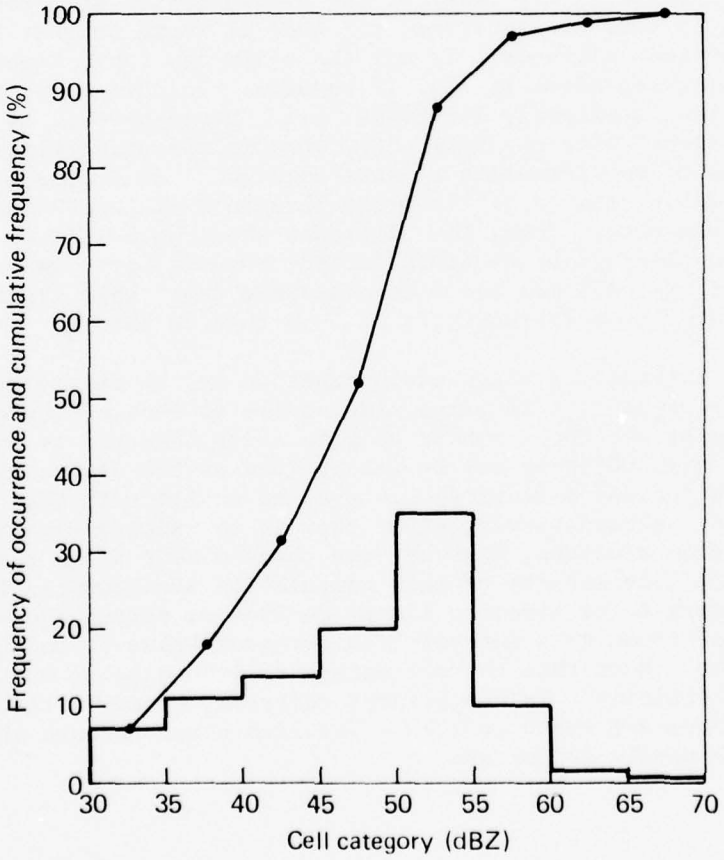

Fig. 15 Distribution of Number of Cells by Category for Altitude Interval of 0 to 2 km

observed during the summer. It should be emphasized that these distributions were determined from data taken over a large area (radius of 75 nmi) and represent the probabilities of occurrence for rains of given intensities anywhere within the area of observation but not at any given point as is the case with rain gauge measurements. Thus, a direct one-to-one comparison is not possible. Some transformation from point to area statistics must be assumed or calculated.

HEIGHT DISTRIBUTIONS OF CELLS

The distributions of cell heights by category are also quite useful in that they indicate the altitudes to which rain cells of given intensities on the ground may be expected to extend. Figure 16 shows the results for three percentage values. For example, for cells in the 45- to 50-dBZ category, 90% of the cells extended to 4 km altitude but only 10% reached 7.7 km. Note that the intensity or reflectivity level of the precipitation at altitude is not known in this presentation; all that is known is that the cell extends to that altitude. If all the cells are taken together, the distribution shown in Fig. 17 results. In this case, the interpretation is slightly different; i.e., given that it is raining at ground level with <u>any</u> intensity, what is the probability of precipitation of <u>any</u> intensity at some altitude? It should be remembered, however, that a reflectivity threshold of 30 dBZ was imposed on the data. Thus, the altitudes shown here will be lower than those observed by an aircraft, for example, or a radar where the top of the cell was based on a minimum detectable signal level corresponding to a reflectivity of less than 30 dBZ.

An interesting piece of information may be determined using the number of ROG and of virga class cells at each altitude. The percentage of the total number of rain cells observed at an altitude that are ROG cells may be interpreted as the percentage of rain cells (of any intensity) observed at an altitude that reach the ground. Alternatively, given that it is raining with some intensity at an altitude, what are the chances that it is raining on the ground? The results of this calculation are shown in Fig. 18. There appears to be almost a linear decline of percentage with increasing altitude to a more-or-less constant value around 50% at 10 to 13 km. Note that the percentage at ground level must be 100% by definition. In the present analysis, however, the first altitude interval was 0 to 2 km. The line drawn through the data points was simply fit by eye.

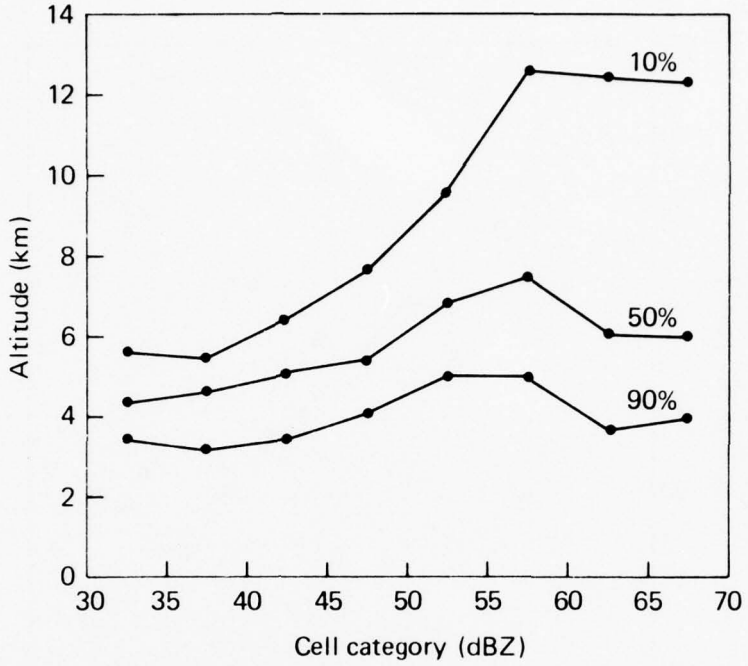

Fig. 16 Probability of a Cell of Given Category Extending to an Altitude

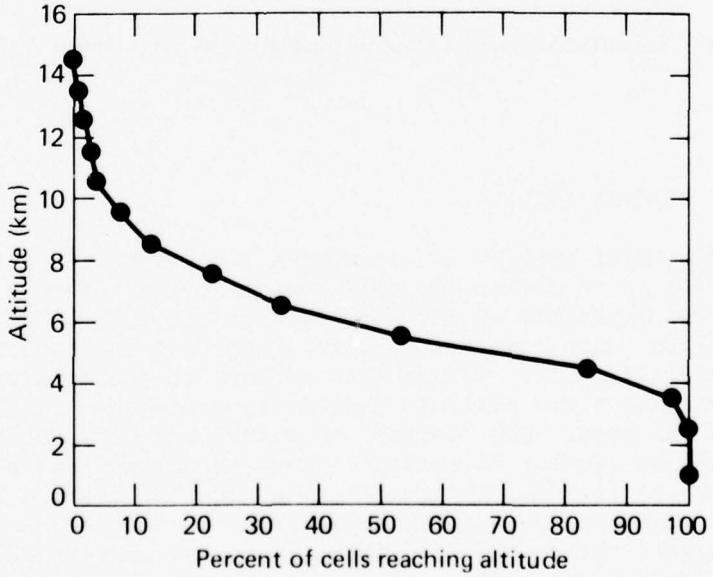

Fig. 17 Percent of Cells Reaching an Altitude Regardless of Cell Category

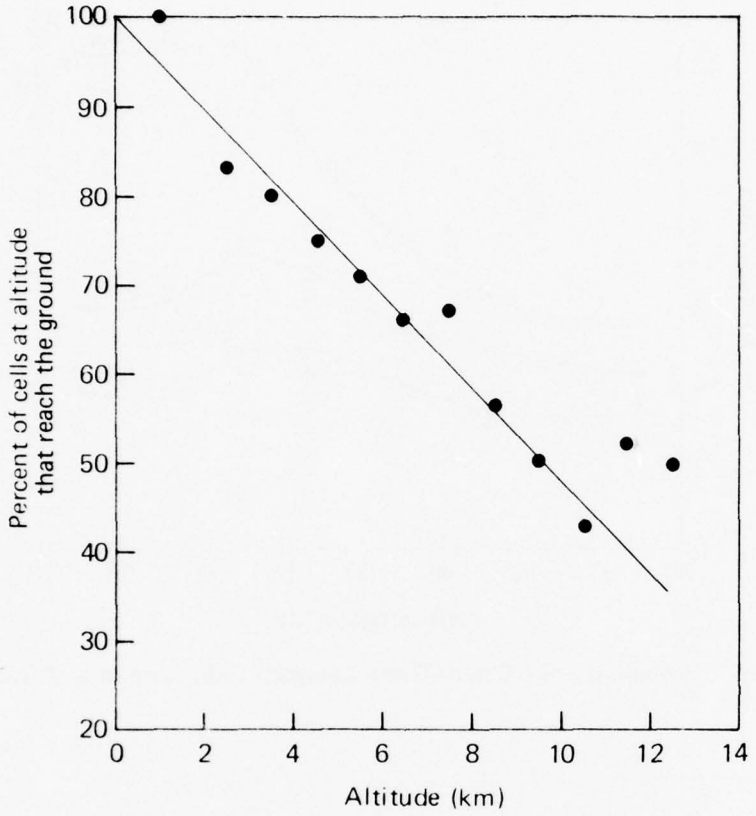

Fig. 18 Percent of Cells Observed at Each Altitude that Reach the Ground

DISTANCE BETWEEN CELLS

The first problem in attempting to analyze the distance between cells is to define the cell center itself. Referring to Fig. 1, the locations of the core reflectivity were plotted for each cell for each sweep of a scan. Note that the core location varies with altitude. Rather than attempt to define a complex cell center that was altitude dependent, a simple straightforward approach was used. The "center" of a cell was defined to be the center of the cluster of core locations as determined by eye, using plots such as Fig. 1. The center is an eyeball average location for all altitudes. Distances between the centers were then measured for all cells, ROG and virga, taken two at a time. As described earlier, the PPI sector scans used in the individual cell

statistics mode of operation were 60° or greater in azimuth. This finite azimuthal, or areal, coverage limits the maximum distance between cells that can be observed and measured. It was felt that the lower end of the resulting frequency distribution curves would not be significantly affected. That is, the smaller distances, which are of interest, lie well within the dimensions of the area covered.

The frequency distribution and cumulative frequency of cell spacings are shown in Fig. 19 where the spacing increment is 2 nmi (3.7 km). The curves do not follow a simple mathematical function. This is not surprising in light of the qualifications to the data discussed above. The most probable distance is around 12 nmi (22 km) with a median value of 18 nmi (33 km). Again, because of the bias in the population of spacings or lack of very high spacing values, the median is certainly too low, but the mode should not be affected significantly.

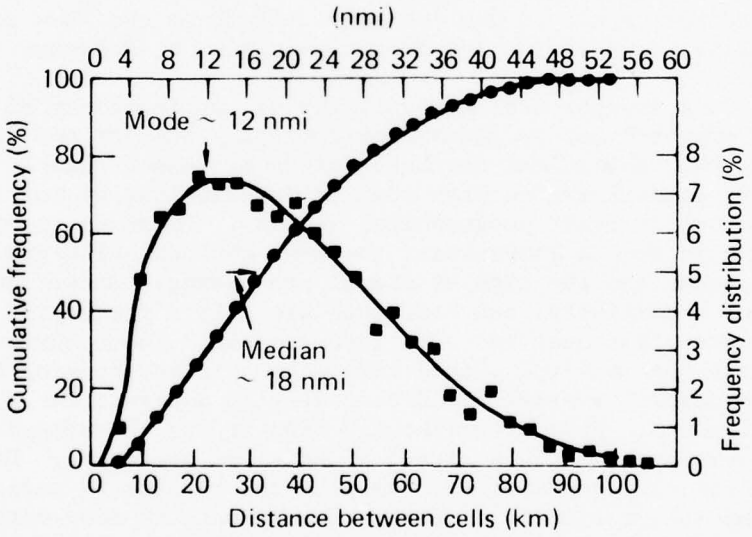

Fig. 19 Distribution of Distance between Rain Cell Centers

5. COMPARISON WITH PREVIOUS INVESTIGATIONS AT OTHER GEOGRAPHICAL LOCATIONS

Two approaches have been used in the past to characterize the attenuation and interference conditions for various geographical locations: the direct method, where the temporal statistics of attenuation and interference are measured at a number of specific locations representing different climatological regions; and the indirect method, where the statistical characteristics or models of the precipitation elements causing the propagation effects are determined.

In the indirect method, the assumption is made that the character of a particular type of precipitation element, such as a thunderstorm, remains essentially constant from one locale to another and only the frequency of occurrence of the particular element varies with geographical location. Thus, the need for extensive statistical studies at many locations is eliminated. This indirect approach was the major effort in the NASA Communications Link Characterization Program outlined by Eckerman (Ref. 3).

Some insight into the validity or applicability of this indirect approach may be gleaned by comparing the present data concerning the statistical characteristics of summer rain in the mid-Atlantic coastal region with similar descriptions by earlier investigators in other geographical regions. There are many obvious pitfalls in such a comparison, the most obvious being the difference in equipment and the type of signal processing. Radar wavelength, receiver sensitivity, and beamwidth are only a few of the equipment differences that must be taken into account. The technique used to determine the received signal level also varies, ranging from step gain to digital averaging and recording in discrete range resolution elements. Another difference lies in the characterizing parameters used in the statistical modeling procedure. Depending on the ultimate application, the data and results by various investigators are cast in different forms that, in many cases, are not comparable. Finally, there is the difference in target population. Some investigators restrict their study to thunderstorms while others, such as in the present study, make no distinction between rainstorms with and without thunder. This noncommonality of the subject population is perhaps the most serious, since it is extremely difficult if not impossible to estimate the effect of the differences on a comparison after the fact. The effects of beamwidth and radar wavelength, for example, on the resolution and

accuracy of the data are known or can be estimated in a gross sense. However, this is not the case when the criteria used in selecting the rain cell population are different or unknown.

Despite these difficulties and qualifications, the comparison of results is useful if only to indicate first-order trends or to show potential variations leading to broad design bounds. It is with this in mind that the present data are compared with those produced by earlier experimental programs albeit for different applications.

Table 1 summarizes experimental conditions, equipment characteristics, observational techniques, and types of analysis for previous investigations in other geographical areas. The cited references present statistical descriptions of one or more cell parameters in a manner similar to that in the present analysis. In a few cases, the manner in which the data were originally presented was changed to the common presentation given here. An attempt is made to preserve the terminology used by the different authors to describe the type of precipitation studied. Actual quotes are included where the description is somewhat subjective as in the case of the "prominent" echoes of Schleusener and Grant (Ref. 17) or "all inclusive" as in Hudlow (Ref. 18). As noted above, the population used in the analysis has a great effect on the statistical results. Additional comments concerning qualifications to the data by individual authors as they affect the comparisons for particular parameters are given in the discussion that follows.

CORE REFLECTIVITY

Profiles of the median core reflectivity factors are presented in Fig. 20. Note that the identification of the curves in this figure and in all subsequent comparisons is in terms of the geographic location where the observations were made and the identification letter from Table 1. The number of cells used in the statistical description is also shown. The profiles are of the

---

Ref. 17. R. A. Schleusener and L. O. Grant, "Characteristics of Hailstorms in the Colorado State University Network, 1960-1961," Preprints 9th Radar Meteorology Conference, American Metorological Society, Boston, 1961, pp. 140-145.

Ref. 18. M. D. Hudlow, "Radar Echo Climatology East of Barbados Derived from Data Collected During BOMEX," Preprints 14th Radar Meteorology Conference, American Meteorological Society, Boston, 1971, pp. 433-437.

Table 1

Summary of Experiment and Equipment Characteristics for Present and Previous Investigations

Ident. Letter	Reference	Location	Equipment	Time of Observation	Observation Technique	Type of Precip. Studied	Type of Analysis	Remarks
j	This report	Wallops Island, VA, mid-Atlantic coast	S band, 0.4° beam, 1 μs pulse	May-Aug 1973	PPI series, digital processing of P_r from 871 range bins	All rain showers within 75-nmi radius at half-hour intervals	Profiles of mean and median core reflectivities Distribution of core reflectivities at altitude Distribution of echo heights Height of maximum reflectivity Distribution of reflectivity ratio Cell spacing Distributions of the eccentricity of cell contours Distribution of cell orientation Distribution of cell areas	No correction for attenuation needed. Correction made for O_2 absorption. Frequency diversity for sample independence
d	Ref. 19*	New England	CPS-9, X band, 1° beam, 5 μs pulse	1956-1957	PPI series for echo height with 5-dB step gain at lowest elevation angle for reflectivity, generally 0° elevation	Investigation restricted to cells with and without hail	Distribution of echo heights Distribution of core reflectivities at lowest elevation angle, generally 0°	No correction for attenuation
e	Ref. 14	New England	CPS-9	1957-1958 "thunderstorm season"	PPI series with 5-dB step gain at each elevation angle	Thunderstorms with and without hail and tornadoes	Profiles of median core reflectivity for rain and hail Distribution of core reflectivity at series of altitudes Distribution of height of maximum reflectivity Distribution of reflectivity ratio	No correction for attenuation
a	Ref. 20*	Western Nebraska	X band tracking radar, S band acquisition radar	May-Aug 1969	PPI series with digital voltmeter measurement of P_r	"Hailers and non-hailers"	Profiles of median core reflectivities for hailers and non-hailers at X and S band	S band data 7 dB low per author

Table 1 (cont'd)

Ident. Letter	Reference	Location	Equipment	Time of Observation	Observation Technique	Type of Precip. Studied	Type of Analysis	Remarks
f	Ref. 21*	Alberta, Canada	X band 0.75° vertical and 4° horizontal beam, 5-μs pulse	Jul, Aug 1957	PPI, constant altitude PPI	Rain with and without hail	Distribution of echo heights Seasonal variability	Limited number of days (5). No mention of attenuation correction. No reflectivity data
b	Ref. 22*	Southwestern Ohio	TRS-10 height finder, X band, 0.7 × 2.0° beam, 1-μs pulse	Summer 1947	RHI series	Thunderstorms	Maximum vertical height	Heights measured for all convective type storms >25 000 ft, not restricted to thunderstorms
l	Ref. 23*	Leningrad, USSR	Unknown	Summer 1962	RHI	Rain showers and thunderstorms	Distribution of maximum vertical height Distribution of height of maximum reflectivity Distribution of maximum cell reflectivity	
g	Ref. 24*	Miami, Florida	MPS-4 4.6-cm height finder	May 1958-June 1970	RHI series	"All precipitation echoes"	Distribution of echo heights for various quadrants and time of year	Shows effects of land versus water
n	Ref. 25*	New England	CPS-9	Jan, Jul 1957 Jan, Jul 1958	RHI series w/gain steps	"Small scale cellular convection"	Distribution of cell heights Distribution of cell spacings	Small-scale convective cells
c	Ref. 26*	Eniwetok	CPS-9	Apr 1960	PPI photographs	Rain showers	Distribution of shower sizes	No mention of attenuation correction
i	Ref. 15	Texas	CPS-9	1959-1960	PPI series with 4 to 7 dB step gain at each altitude	Thunderstorms with and without hail and tornadoes	Profiles of median and quartile core reflectivities for rain cells and hail storms Distribution of echo heights Height of maximum reflectivity distribution	Assumed radar constant. No mention of attenuation correction

Table 1 (cont'd)

Ident. Letter	Reference	Location	Equipment	Time of Observation	Observation Technique	Type of Precip. Studied	Type of Analysis	Remarks
h	Ref. 18	Barbados	MPS-34 X band 0.5- and 5-μs pulse, 1° beam	Jun, Jul 1969	PPI series with step gain	"All inclusive"	Distribution of echo dimensions Distribution of echo spacings Distribution of echo heights	Observations divided into two categories based on "state of the weather" as disturbed and undisturbed. No mention of attenuation correction
m	Ref. 17	Northeastern Colorado	X band, characteristics unknown	May-Aug 1961	PPI series with attenuation	"Prominent" echoes, both rain and hail producing cells	Distribution of echo heights	No mention of attenuation correction
k	Ref. 27*	North Dakota	M-33	May-Aug 1972	PPI photographs	Rain showers	Distribution of shower size	

* Ref. 19. R. J. Donaldson, "Analysis of Severe Convection Storms Observed by Radar – II," J. Appl. Meteorol., Vol. 16, 1959, pp. 281-287.

Ref. 20. E. I. Boyd and D. J. Musil, "Radar Climatology of Convective Storms in Western Nebraska," Preprints 14th Radar Meteorology Conference, American Meteorological Society, Boston, 1970, pp. 433-437.

Ref. 21. R. H. Douglas and W. Hitschfeld, "Studies of Alberta Hailstorms, 1957," McGill University, Stormy Weather Research Group, Science Department Report MW-27, 1958.

Ref. 22. H. R. Byers and R. R. Braham, The Thunderstorm – Report of the Thunderstorm Project, U.S. Government Printing Office, Washington, DC, 1949.

Ref. 23. E. M. Salman and K. S. Zhupaklien, "Some Results of Radar Investigations of the Vertical Structure of Showers and Thunderstorms," Glavnaia Geofizicheskaia Observatorua, Trudy, No. 159, 1967, pp. 59-64, Translation AD 667403.

Ref. 24. H. W. Hiser and R. R. Adt, "Precipitation Echo Heights in South Florida," Preprints 9th Radar Meteorology Conference, American Meteorological Society, Boston, 1961, pp. 90-95.

Ref. 25. R. E. Newell, "Some Radar Observations of Tropospheric Cellular Convection," Preprints 8th Radar Meteorology Conference, American Meteorological Society, Boston, 1960, pp. 315-322.

Ref. 26. A. S. Dennis and F. G. Fernald, "Frequency Distribution of Shower Sizes," J. Appl. Meteorol., Vol. 2, 1963, pp. 767-769.

Ref. 27. J. R. Miller, A. S. Dennis, J. H. Hirsh, and D. E. Cain, "Statistics of Shower Echoes in Western North Dakota," Preprints 16th Radar Meteorology Conference, American Meteorological Society, Boston, 1975, pp. 391-396.

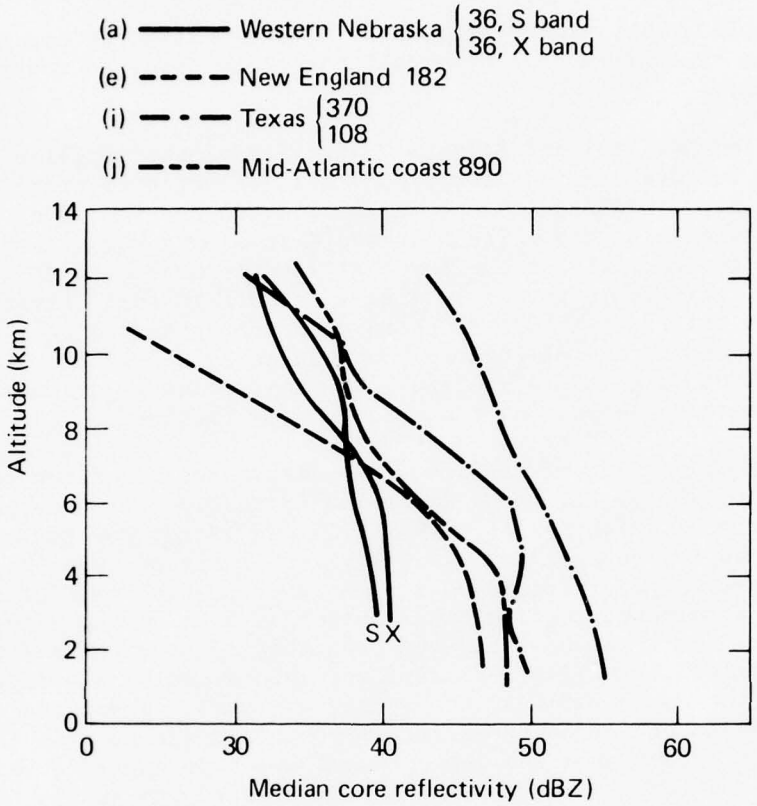

Fig. 20 Profiles of Median Core Reflectivity Factor for Various Geographical Locations (identifying letters indicate references in Table I)

median values of the observed cell reflectivities at each altitude, with the exception of the New England data of Donaldson (Ref. 14). He includes reflectivity values of zero at altitudes above the echo top in his distributions; hence, the median values shown are smaller and the falloff with altitude more severe than if only the observed reflectivities were included. This effect becomes more pronounced with increasing altitude since the number of rain cells reaching these altitudes becomes smaller.

The data by Boyd and Musil for Western Nebraska (Ref. 20) were taken simultaneously at X and S band. The authors indicate in their paper that the S band data were 7 dBZ low and this correction has been added to the profile. An indication of a year-to-year variation is shown by the two sets of data for Texas by Inman and Arnold (Ref. 15). The difference is particularly

noticeable at the higher altitudes. The mid-Atlantic coast profile was taken from Fig. 6 for all the cells observed regardless of category.

The New England, Atlantic coast, and Texas profiles have similar features, a relatively constant reflectivity profile around 45 to 50 dBZ up to 4 to 6 km altitude and then a steady falloff with altitude. The Nebraska data show a significantly smaller reflectivity at the lower altitudes, around 40 dBZ, extending again to roughly 6 km with a falloff in reflectivity at higher altitudes. Note that there does not appear to be a pronounced knee in any of the median profiles as is typical when hail is involved (e.g., Refs. 14 and 15). This point is discussed later in the section concerning the reflectivity ratio.

A comparison of the frequency distributions of the core reflectivity at 1.5, 6, and 9 km are shown in Figs. 21 through 23. Again, the distributions from Refs. 14 and 19 for New England include zero reflectivity values at altitudes higher than the echo top height. The distribution at 1.5 km is probably not affected by this procedure, and the distribution at 6 km may be affected slightly. At 9 km, however, the frequency of occurrence for a given reflectivity (Fig. 23) is lower than would be the case if only the observed reflectivities had been used. Inman and Arnold (Ref. 15) do not present complete frequency distributions at altitudes but rather show the low, median, and high quartile reflectivity profiles. The three values of reflectivity at 25, 50, and 75% were taken from these profiles at the three altitudes.

At 1.5 km (Fig. 21), the New England and Atlantic coast distributions are quite similar. The widths of the distributions between the 25 and 75% points are surprisingly similar for all three locations, ranging from 10 to 12 dBZ. At 6 km, the widths of the distributions are somewhat larger, ranging from 12 to 17 dBZ.

REFLECTIVITY RATIO

As was noted above, the median reflectivity profiles for rain do not exhibit any appreciable knee or maximum at altitude. This is further illustrated in Fig. 24 where the distribution of the reflectivity ratio is shown for the New England and Atlantic coast locations. A ratio of one indicates that the maximum core reflectivity was located at the ground or in the first altitude increment. This is the case 50% of the time for the New England data, with 75% of the cells having a ratio of less than three. In the case of the Atlantic coast data, the sorting bin size was two,

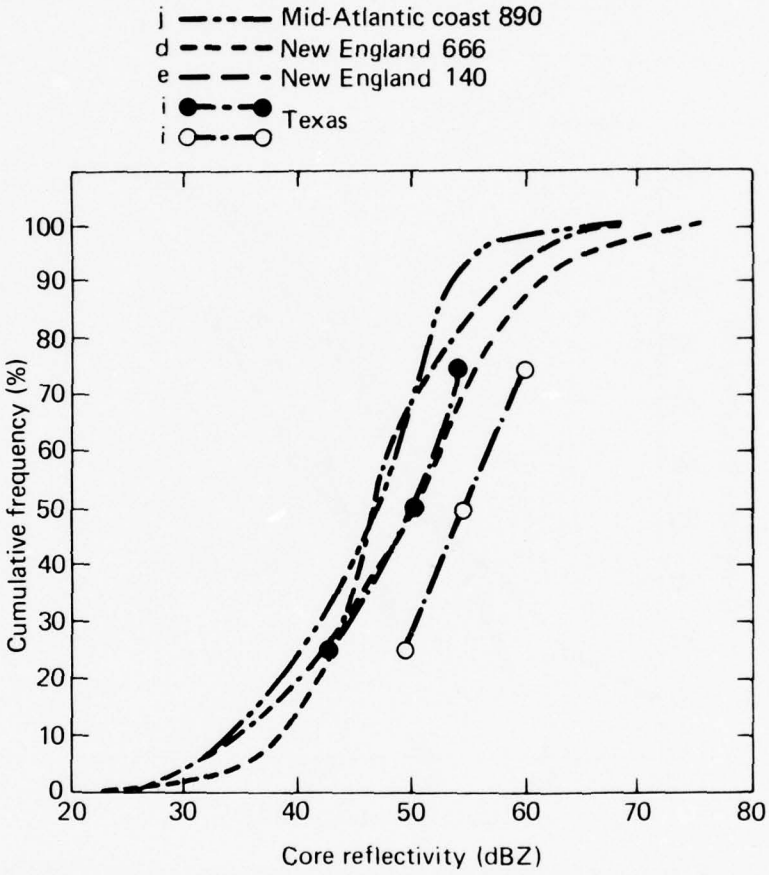

Fig. 21 **Frequency Distributions of Core Reflectivity at 1.5-km Altitude for Various Locations. The Texas data with solid symbols were taken in 1959, open symbols in 1960.**

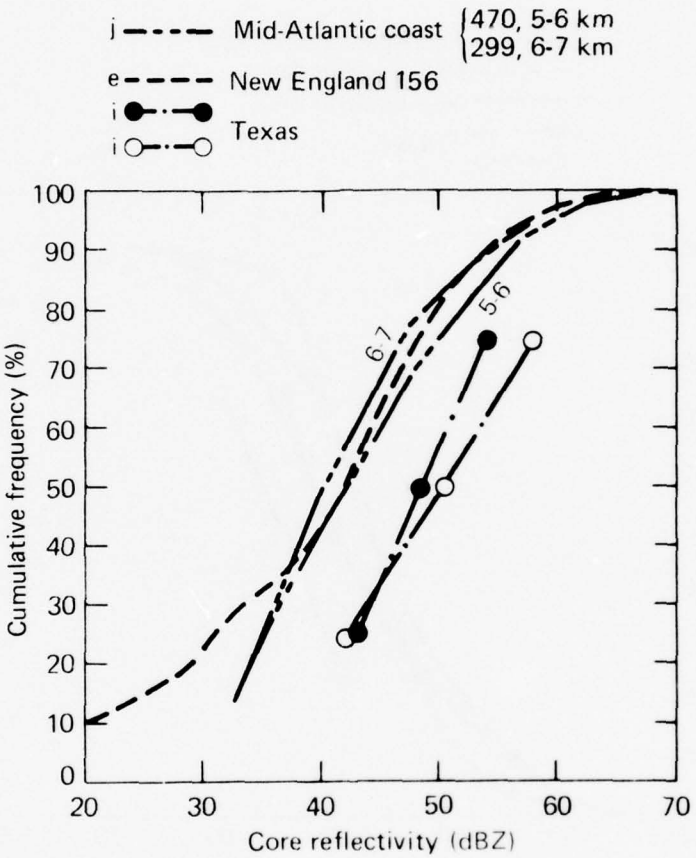

Fig. 22 **Frequency Distributions of Core Reflectivity at 6-km Altitude for Various Locations. The Texas data with solid symbols were taken in 1959, open symbols in 1960.**

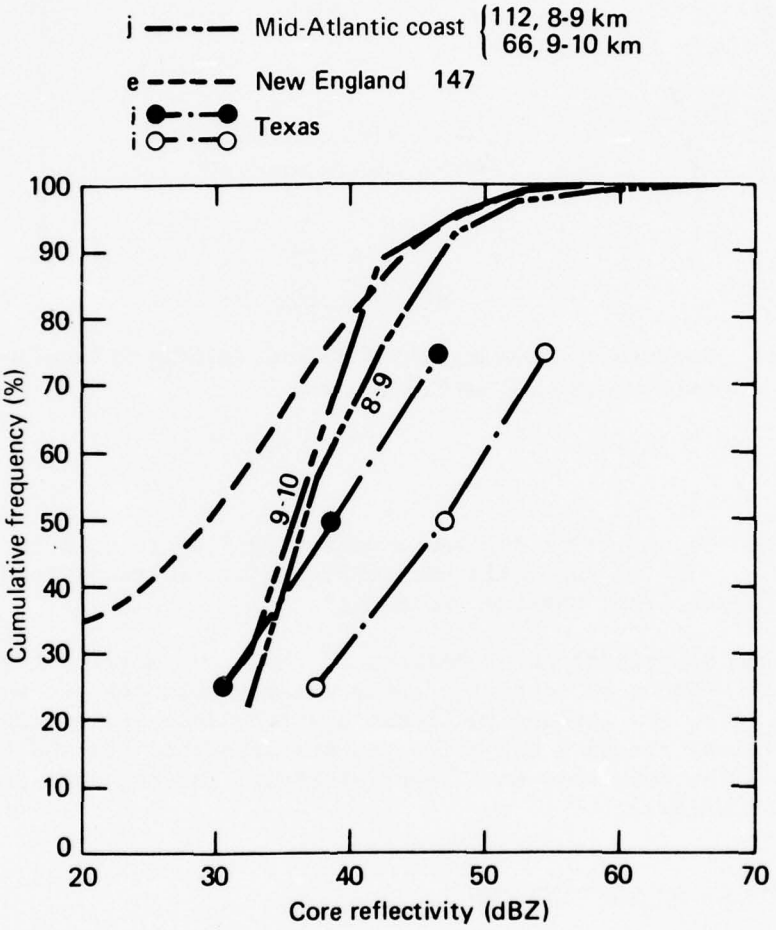

Fig. 23 Frequency Distributions of Core Reflectivity at 9-km Altitude for Various Locations. The Texas data with solid symbols were taken in 1959, open symbols in 1960.

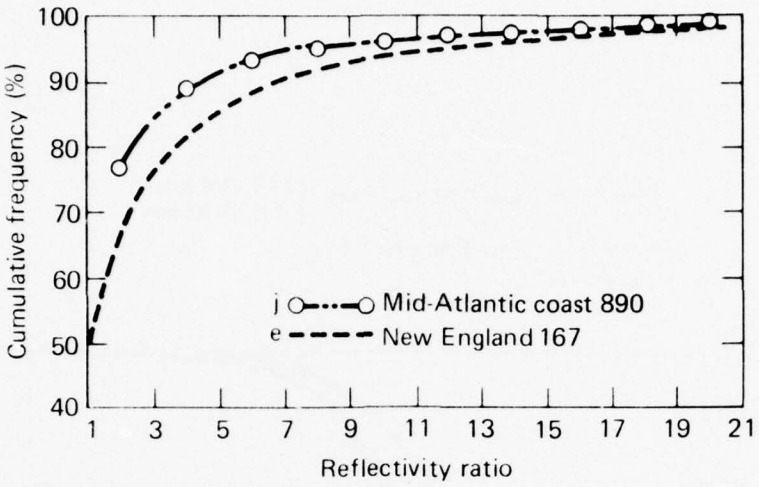

Fig. 24 Comparison of Distributions of Reflectivity Ratio for New England and Mid-Atlantic Coast Rain Showers

i.e., the increments in the ratio were 1 to 3, 3 to 5, 5 to 7, etc. Again, over 75% of the cells had reflectivity ratios of less than three (in the first sorting increment).

The distributions of heights of the maximum reflectivity for cells that have a reflectivity ratio greater than one are shown in Fig. 25. The New England and Texas distributions are similar with median values around 4 km, while the distributions for the Atlantic coast and the USSR show much lower altitudes for the same probability of occurrence.

DISTRIBUTION OF ECHO HEIGHTS

The frequency distributions of maximum echo height for a variety of locations are shown in Fig. 26. The population of cells used for the Atlantic coast distribution consisted only of cells that reached the ground. Other investigators do not make this distinction. In addition, a core reflectivity threshold of 30 dBZ was imposed on the present data, as was discussed earlier. Therefore, the distribution shown for the mid-Atlantic coast is more properly the height of the 30-dBZ core reflectivity. If the echo height corresponding to the limit of radar sensitivity had been used, as was the case with other investigators, the distribution would be considerably higher, i.e., a higher altitude for a given frequency of occurrence.

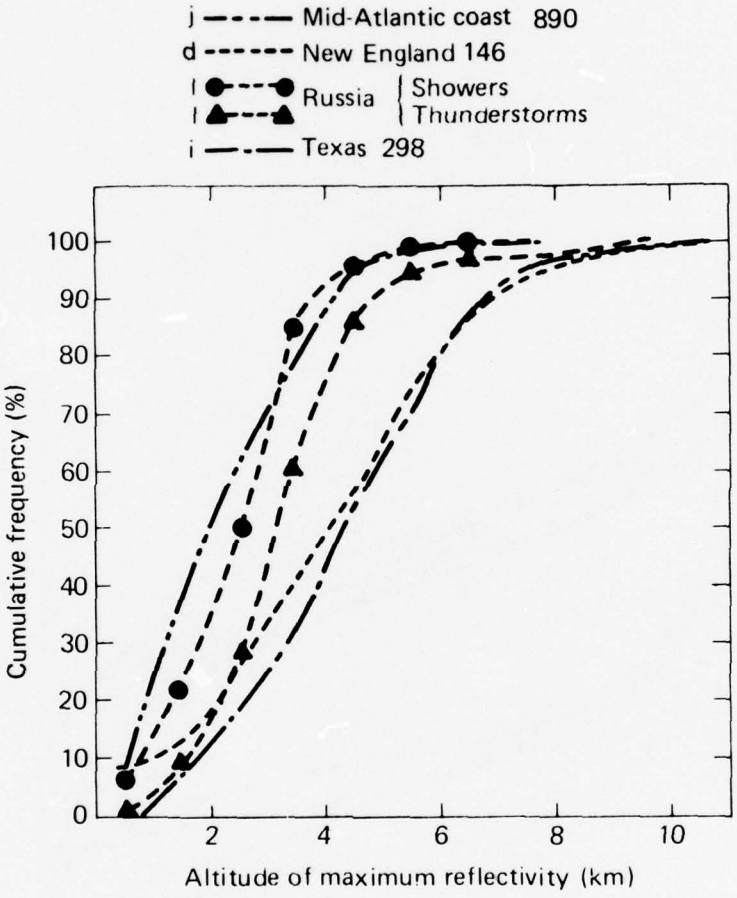

Fig. 25 Altitude of Maximum Core Reflectivity for Various Locations

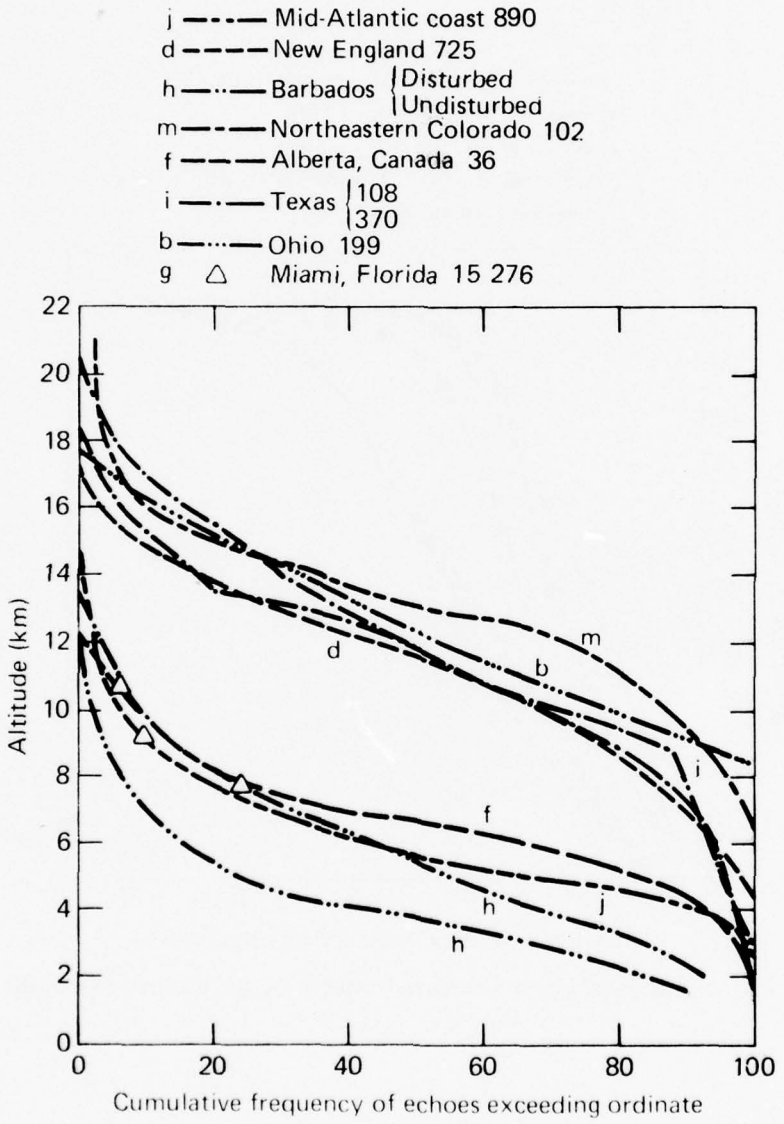

Fig. 26 Maximum Echo Height Distributions for Various Locations

The echo height distribution for Ohio from the Thunderstorm Project includes only echoes above 25 000 ft (7.6 km). As such, the frequency distribution is more like a conditional probability, i.e., the probability of a cell reaching some altitude or above given that it has already reached 25 000 ft. If all echoes had been included in the population, the distribution would be lower than that shown in the figure. Schleusener and Grant (Ref. 17) included only "prominent" echoes in their cell population taken in Eastern Colorado. Presumably these are the larger and stronger echoes. If all echoes had been included, such as was the case with Hudlow (Ref. 18) in the Barbados and Hiser and Adt (Ref. 24) in Florida, the distribution of echo heights again presumably would be lower than shown.

In their report on echo heights in Miami, Florida, Hiser and Adt (Ref. 24) quote frequencies of occurrence for only three altitudes: 25 000, 30 000, and 35 000 ft. However, the percentages are not conditional as was the case with the Ohio data. All precipitation echoes were included in the population on which the percentages were based.

Hudlow (Ref. 18) divided his data for the Barbados taken during BOMEX into two categories based on the state of the tropical oceanic environment: "the disturbed state, manifested by synoptic-scale disturbances" and a "relatively undisturbed state, manifested by 'normal' trade-wind cumuli." In the undisturbed state, the median echo top is about 2 km lower than in the disturbed state.

Despite the qualifications discussed above, the distributions of echo heights show a gross correlation with climatic region. The CCIR (Comité Consultatif International des Radiocommunications) report (Ref. 28) presents five rain climatic zones based on the distribution of rainfall rates. The regions may be classed as maritime subtropical, continental temperate, maritime temperate, Mediterranean, and desert. Echo tops in the maritime subtropical region exhibited by the Barbados, Florida, and mid-Atlantic coast data appear to be lower than in the continental temperate region. (Wallops Island is near the boundary between the maritime subtropical and continental temperate zones.) In the continental temperate region, where all the other observing stations are located, the distributions of echo tops are quite similar.

Ref. 28. "Radiometeorological Data," CCIR Report 235-2, 1974, pp. 92-112.

DISTANCE BETWEEN CELLS

The distributions of the distance between cell centers are compared in Fig. 27 for three locations. Hudlow (Ref. 18) found that the interspacing distributions for the Barbados rain cells were remarkably similar for the disturbed and undisturbed periods. There is a striking difference, however, between the Barbados distribution for rain cells over the open ocean in the maritime subtropical region and for those over land in the continental temperate region, i.e., the New England and mid-Atlantic coast distributions. The two latter distributions are similar to each other, with median cell separations around 30 to 35 km compared to the Barbados median of 15 km. Although the Barbados distribution is more highly peaked at low separation distances, its tail extends to longer distances than do those of the other two distributions. This may be the result of a larger observation area where longer distances can be measured. The point was discussed in an earlier section on cell separation and the limitations to the Wallops Island data resulting from the PPI sector scanning technique used in the experiment. Despite these qualifications, it appears that the cells over the subtropical ocean are smaller, do not extend as high, and are more closely spaced than those over land in the temperate regions.

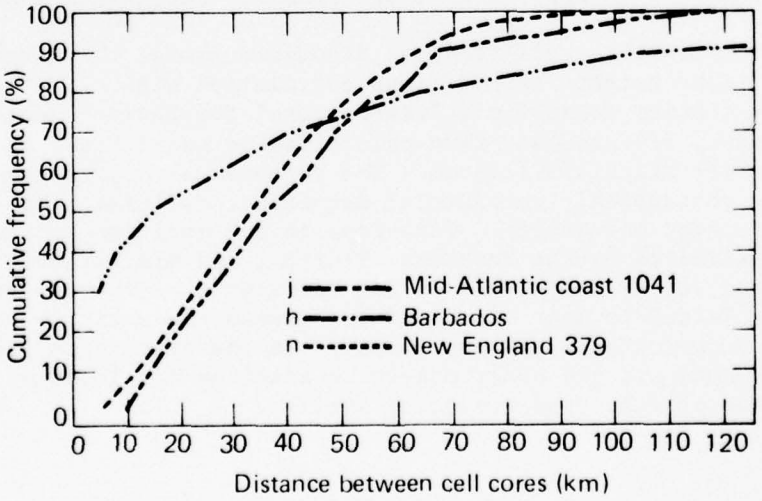

Fig. 27 Frequency Distributions of Distance between Rain Cell Centers

FREQUENCY DISTRIBUTIONS OF CELL SIZES

It has been suggested by several authors that the number of shower echoes decreases exponentially as a function of echo size. Dennis and Fernald (Ref. 26) studied some 2400 showers observed on a CPS-9 (3-cm) radar at Eniwetok Atoll. On an hourly basis the radar echoes on PPI photographs were counted, measured, plotted on semilogarithmic paper, and fitted to an exponential form by linear regression. A similar procedure was followed using data from central Illinois, England, and picket ships off the west coast of the United States. In all cases the correlation coefficients were high, ranging from 0.92 to 1.00. The slopes of the distributions ranged from -0.21 to -0.38 km^{-1}. Presumably the size of the radar echo corresponded to the minimum detectable signal level at whatever range and altitude the echo occurred. The authors did not attempt to subdivide the data according to altitude, range, or shower intensity, i.e., core reflectivity.

A similar analysis was performed by Miller et al. (Ref. 27) on data collected in western North Dakota using an M-33 (10-cm) radar during the summer of 1972. Over 2700 "well defined convective storms" were recorded on PPI photographs. The slope of the distribution was -0.35 km^{-1} and the correlation coefficient was 0.97. Again, no subdivision according to the strength of the storm, range, or altitude was attempted. The data were subdivided by time of day and by day. Some variation in the distribution slope was found for morning showers versus late afternoon and evening showers. No seasonal trend was evident.

The present data were examined to determine if the exponential form of the distribution is still applicable when the rain shower population is subdivided according to altitude and/or reflectivity contour level. In the first instance, all the cells in the altitude interval of 0 to 2 km regardless of category (e.g., core reflectivity) were considered. Figure 28 shows the frequency distribution in a manner similar to that used in Refs. 26 and 27. An exponential distribution appears reasonable with a slope of -0.36 km^{-1}.

In the second instance, cell diameters at the same contour reflectivity level were considered regardless of altitude. Again, the exponential representation appears reasonable as is shown in Fig. 29 for the 30- to 35-dBZ contour. Data for 35 to 40, 40 to 45, 45 to 50, and 55 to 60 dBZ were also plotted but are not shown. The values of the slopes range from -0.42 to -0.5 km^{-1} and there is no particular pattern with respect to contour value.

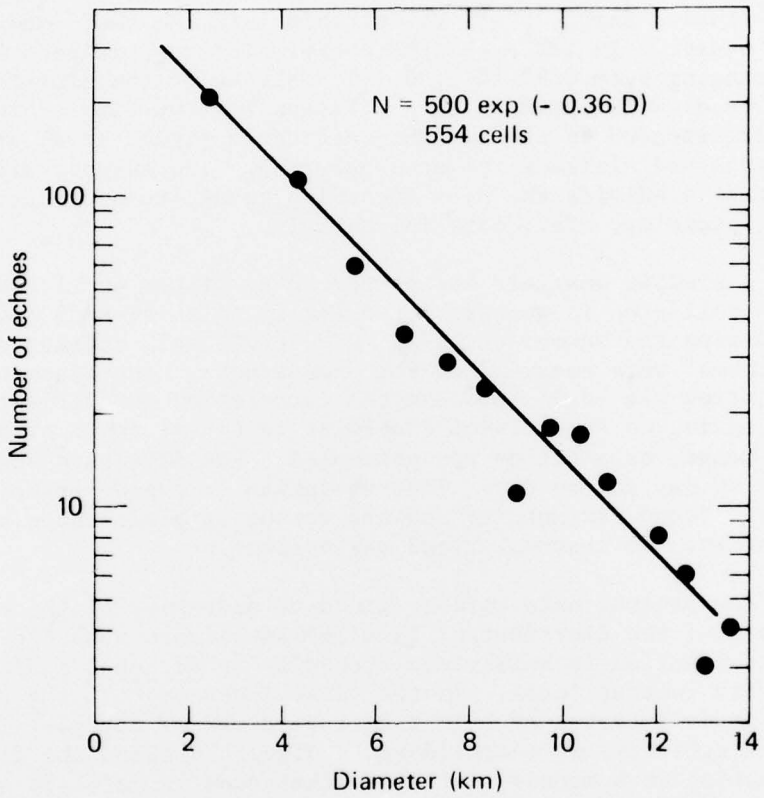

Fig. 28 Distribution of Number of Rain Echoes According to Echo Diameter in Altitude Interval of 0 to 2 km Regardless of Cell Category

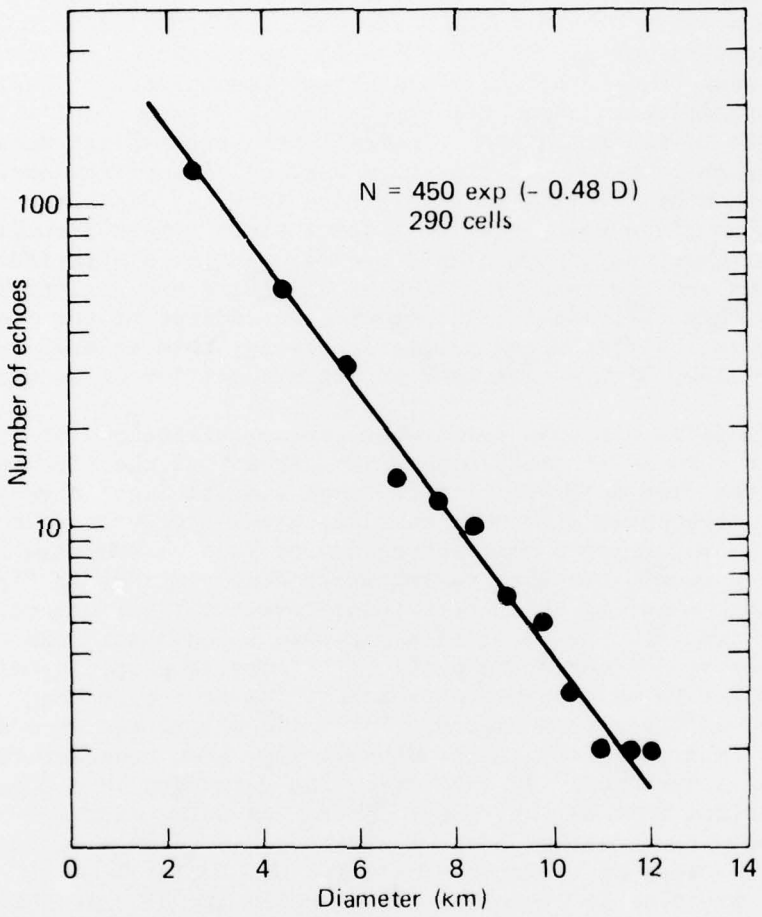

Fig. 29 Distribution of Number of Rain Echoes According to Echo Diameter for 30- to 35-dBZ Reflectivity Contour Regardless of Altitude

6. USE OF STATISTICAL DESCRIPTIONS TO FORMULATE RAIN CELL MODELS

The definition of a rain cell model is highly dependent on the ultimate use of the model. For example, models developed for communications engineers to be used in the design of microwave systems will be entirely different from those needed by hydrologists for agricultural or runoff problems. No one model will be applicable to all situations. However, the statistical descriptions may be combined and used in a variety of applications. Interpretation of the individual distributions was discussed in previous sections where they were described. A method outlined below for constructing rain cell models uses the statistical descriptions and the results of the experimental and analytical program. A rain cell model is considered to consist of the spatial distribution of precipitation (reflectivity) both in area and with altitude along with an estimate of its probability of occurrence.

Consider a simple model where the precipitation at any altitude is not to be exceeded some given percent of the time regardless of the rain at ground level. Such a model might have application in designing a microwave communications link where the attenuation to be encountered some percentage or less of the time is needed. For such a model, the core reflectivity distributions in Figs. 5 and 6 apply, remembering that these cumulative distributions were developed using all the rain cells observed in each altitude increment. Figure 30a shows the profiles of core reflectivity with altitude for three cumulative probabilities of occurrence. The 50% curve is taken from Fig. 6; the 75 and 90% curves were constructed by cross-plotting the data in Fig. 5 at constant frequency of occurrence. In each case, the data have been smoothed. Distributions such as these were determined using data for only those cells that reached a given altitude; no zeros were included in the frequency of occurrence calculations. Thus, we may truncate the profiles at the altitudes to which 50, 75, and 90% of the cells extend in Fig. 17. The profiles above these points are indicated by dashes in Fig. 30a.

For some applications, a simplified linear cell model may be adequate (Fig. 30b). The slope of the reflectivity falloff with altitude (2.5 dBZ/km) was drawn with emphasis on the altitude range in which the cells are expected to occur, e.g., altitudes less than 9 km or so for the 90% profile in Fig. 30a.

Having the profiles of the peak or core reflectivity, we may construct the contours of contant reflectivity using Eq. (2). As an example, we use the median profile from Fig. 30a. From

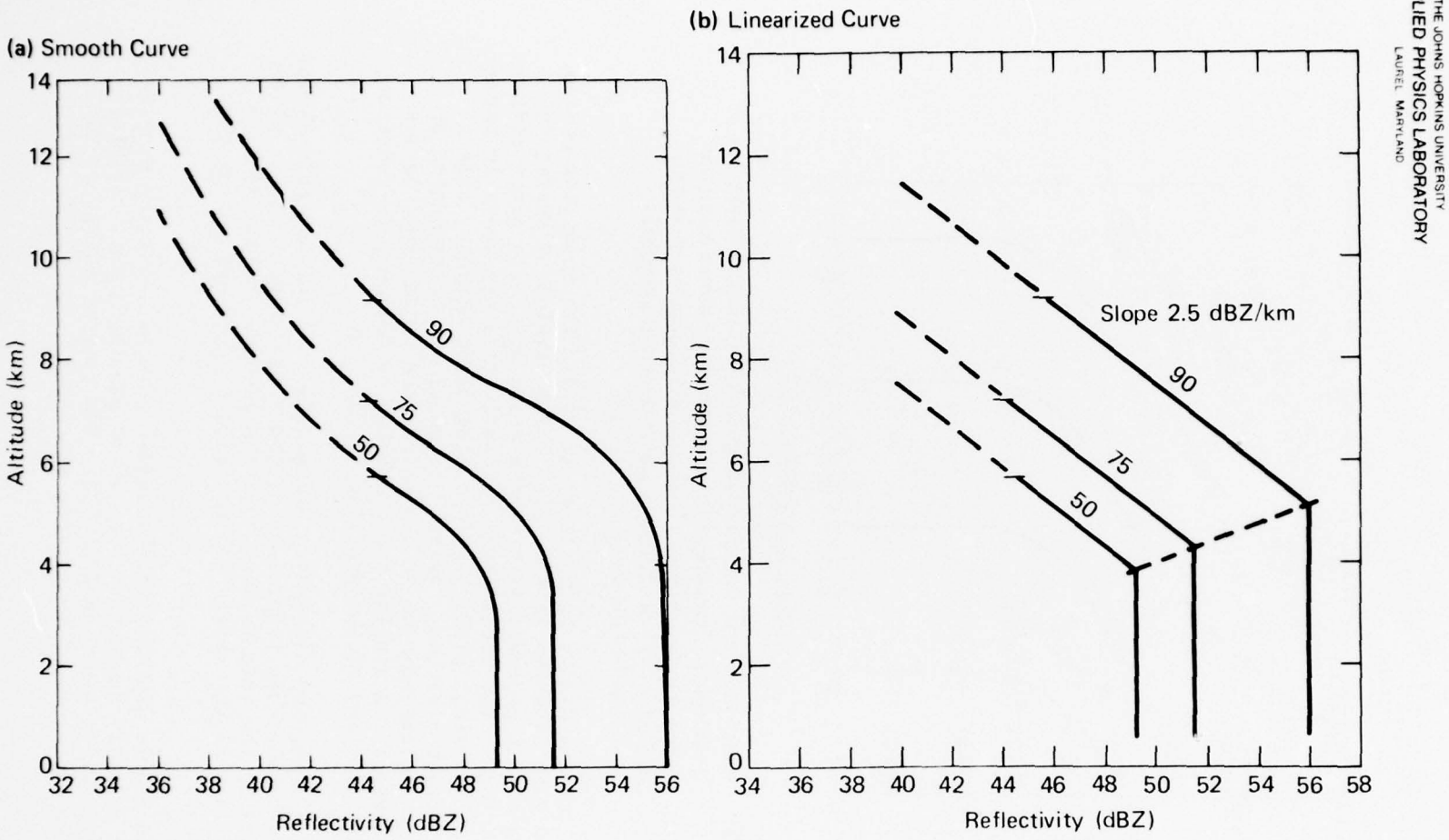

Fig. 30 **Smoothed and Linearized Profiles of Core Reflectivity for Three Probabilities of Occurrence Using All Cells Observed Regardless of Category. The profiles are shown dashed above the altitudes to which cells are expected to extend for a given frequency of occurrence.**

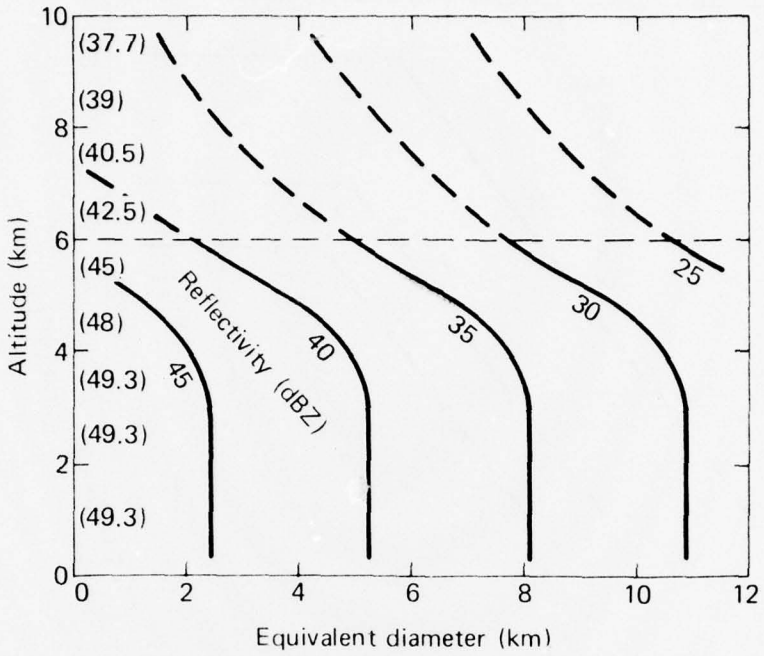

Fig. 31 Model of Median Rain Cell Using all Cells Observed Regardless of Category. The core reflectivity values are shown along the ordinate in parentheses. The reflectivity contours are shown dashed above the altitude to which the cell is expected to extend half of the time.

Fig. 12, let the slope, b, be taken as -2.0. The resulting median cell structure is shown in Fig. 31. The equivalent diameter is that of a circle corresponding to the area, A_c, for a given reflectivity contour. The median peak reflectivities are shown in parentheses for reference along the zero equivalent diameter axis at the appropriate altitude. Again, the model may be truncated at around 6 km, corresponding to the height the median cell is expected to reach. A similar procedure may be followed to construct model cells for any of the profiles in Fig. 30.

The foregoing discussion and models used all the rain shower data at each altitude regardless of the rain category, i.e., without regard to the rain intensity on the ground. Models of rain cells in each of the categories may also be developed using the same method.

In Figure 32a we have the median core reflectivity profiles for each category taken from Fig. 4 and smoothed; the linearized representation is shown in Fig. 32b. The core profiles for 90% cumulative frequency of occurrence are shown in Fig. 33 (a and b)

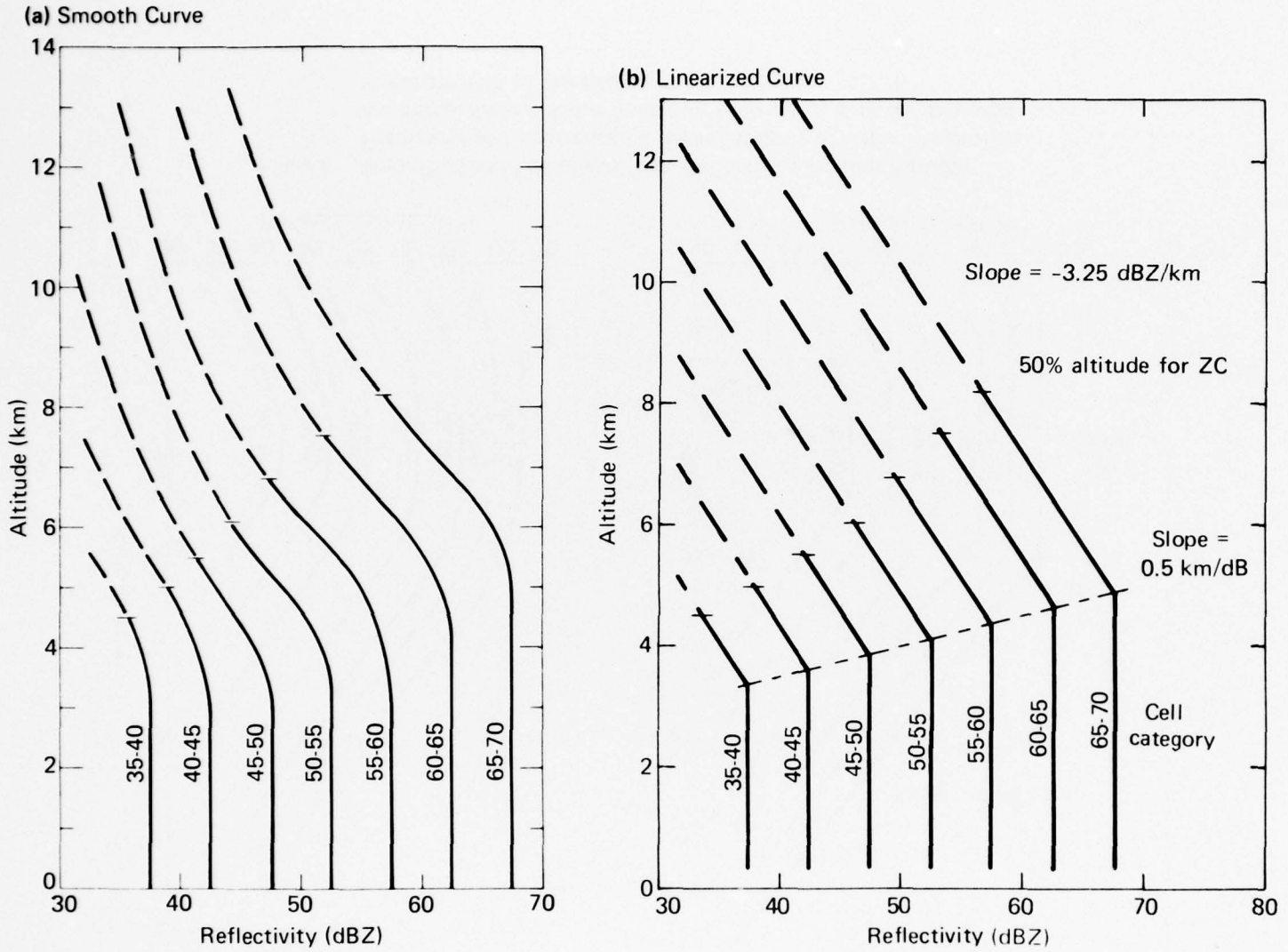

Fig. 32 Smoothed and Linearized Median Core Reflectivity Profiles for Each Category of Cell. The profiles are shown dashed above the altitude to which the cell is expected to extend half of the time.

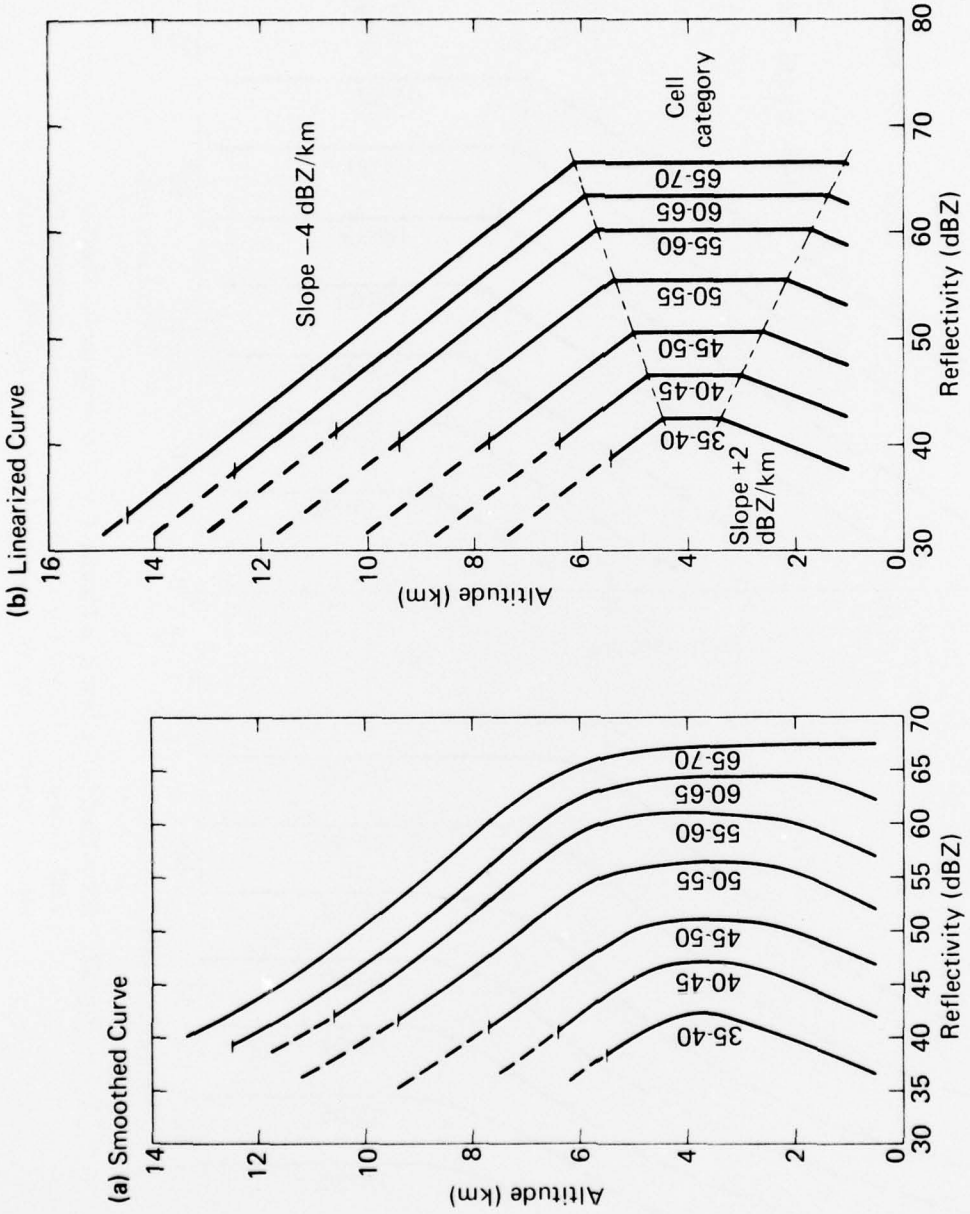

Fig. 33 Smoothed and Linearized Core Reflectivity Profiles for 90% Frequency of Occurrence for Each Category of Cell. The profiles are shown dashed above the altitudes to which cells are expected to extend 10% of the time.

where the values at each altitude were determined by cross-plotting the distributions such as Fig. 2 for each category. Note that the profiles have a distinct knee that gets progressively less apparent with increasing category. The reason for this behavior is evident in the frequency distributions for each category. In Fig. 2, for high cumulative frequencies, the core reflectivities at some altitudes exceed the category values, thus the knee to the profile. At low cumulative frequencies the reflectivities are smaller than the category values at all altitudes above ground level. In other words, if we want a reflectivity profile for some cell category that is not exceeded 90% of the time, we should expect to include those few cells with core reflectivities greater than the ground or category value.

Conversely, for a cell model that will not be exceeded 15% of the time, we will have core reflectivities less than the category values. Further, we would expect this feature to become less apparent with increasing cell category. If it is raining at ground level with a reflectivity in the 65- to 70-dBZ category, the chances are very small that the rain intensity at higher altitudes will exceed this level. On the other hand, if it is raining with an intensity corresponding to a 35- to 40-dBZ category, the chances (or frequency of occurrence) are greater that the rain at altitudes exceeds that at ground level. Thus, the shape of the peak reflectivity profile and the consequent reflectivity contour structure will change as a function of the cell category and the frequency of occurrence chosen. This does not happen, of course, in the case discussed earlier where all the rain data are considered together at each altitude regardless of rain intensity.

The altitude to which each category cell is expected to extend, for a given frequency of occurrence, was taken from Fig. 16. The peak profiles are indicated by dashes above this altitude in Figs. 32 and 33.

As another example of a cell model derived from the statistical characteristics, suppose that we need a model of a rain shower in the 50- to 55-dBZ category that will not be exceeded 90% of the time. Suppose, further, that for our application a linear model is sufficient. From Fig. 33b we have the peak reflectivity profile. Using the above procedure, we construct the contour model. The contours will follow closely the shape of the peak reflectivity profile. The 90%, 50- to 55-dBZ category model is shown in Fig. 34. The slope used in the calculation of contour area was -2.3, from Fig. 12. The probability of occurrence of a 50- to 55-dBZ category rain cell is not included. The 90%, 50- to 55-dBZ model presumes that we have rain on the ground in that category. The probability of occurrence for storms of various categories was shown in Fig. 15. Similar

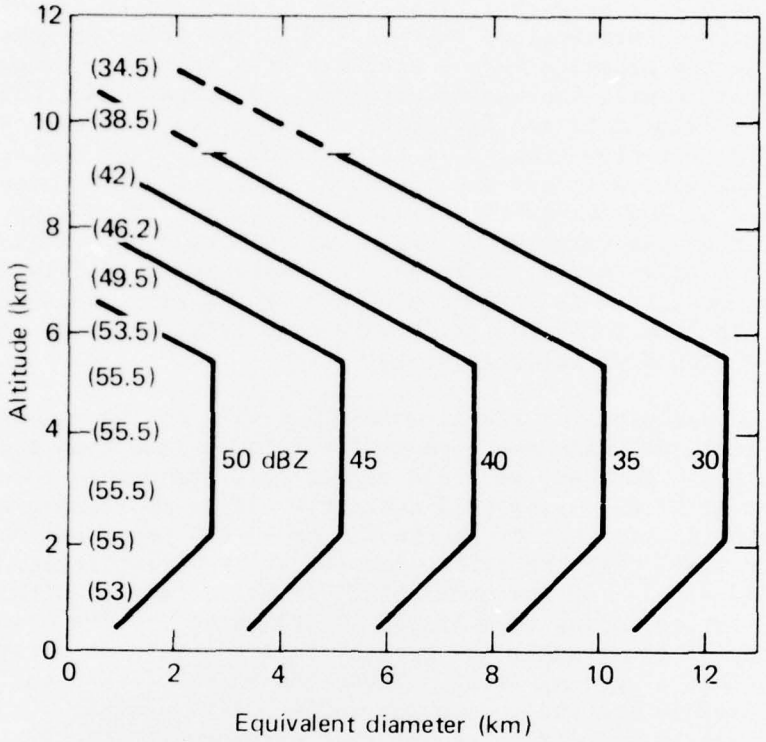

Fig. 34 Model of 50- to 55-dBZ Category Cell that Will Not Be Exceeded 90% of the Time. The core reflectivity values are shown along ordinate in parentheses. The reflectivity contours are shown dashed above the altitude to which the cell is expected to extend 10% of the time.

distributions can be developed for other geographical locations. Knowing the distributions of rain intensities on the ground, we may use the statistical descriptions and modeling procedure outlined above to construct the required cell model, assuming that the statistical descriptions are representative at locations other than in the mid-Atlantic region.

ACKNOWLEDGMENTS

This work was supported by NASA, Goddard Space Flight Center, under NASA/DoD Agreement S-70248AG. The author gratefully acknowledges the help of the APL Radar Atmospheric Physics Group including I. Katz, A. Arnold, R. A. Kropfli, J. R. Rowland, J. Goldhirsh, E. B. Dobson, and F. L. Robison, all of whom took part in the experiment and portions of the analysis. Also, the author acknowledges the efforts and cooperation of J. C. Howard and the personnel at the Radar Atmospheric Research Facility, NASA/Wallops Station, where the data were taken.

REFERENCES

1. R. K. Crane, "Propagation Phenomena Affecting Satellite Communication Systems Operating in the Centimeter and Millimeter Wavelength Bands," Proc. IEEE, Vol. 59, No. 2, 1971, pp. 173-188.

2. D. C. Hogg and T. Chu, "The Role of Rain in Satellite Communications," Proc. IEEE, Vol. 63, No. 9, 1975, pp. 1308-1331.

3. J. Eckerman, "A NASA Program to Characterize Propagation and Interference for Space Applications," AIAA 4th Communications Satellite Systems Conference, 1972, No. 72-577, AIAA, New York.

4. I. Katz, A. Arnold, J. Goldhirsh, T. G. Konrad, W. L. Vann, E. B. Dobson, and J. R. Rowland, "Radar Derived Spatial Statistics of Summer Rain — Experiment Description," Vol. I, Final Contractors Report, NASA CR-2592, 1975.

5. T. G. Konrad and R. A. Kropfli, "Radar Derived Spatial Statistics of Summer Rain — Data Reduction and Analysis," Vol. II, Final Contractors Report, NASA CR-2592, 1975.

6. "Radar Derived Spatial Statistics of Summer Rain — Appendices," Vol. III, Final Contractors Report, NASA CR-2592, 1975.

7. D. Atlas, "Advances in Radar Meteorology," Advances in Geophysics, Vol. 10, Academic Press, New York. 1964, pp. 318-478.

8. J. S. Marshall and W. Hitschfeld, "Interpretation of the Fluctuating Echo from Randomly Distributed Scatterers: Part I," Can. J. Phys., Vol. 31, 1953, pp. 962-994.

9. P. R. Wallace, "Interpretation of the Fluctuating Echo from Randomly Distributed Scatterers: Part II," Can. J. Phys., Vol. 31, 1953, pp. 995-1009.

10. J. M. Austin and M. R. Shaffner, "Computations and Experiments Relative to Digital Processing of Weather Radar Echoes," Preprints 14th Radar Meteorology Conference, American Meteorological Society, Boston, 1970, pp. 375-380.

PRECEDING PAGE BLANK-NOT FILMED

11. P. M. Austin, "Application of Radar to Measurement of Surface Precipitation," Technical Report ECOM 01472-3, Semi-Annual Report 3, Contract DA 28-043 AMC-01472(E), Massachusetts Institute of Technology, 1967.

12. A. J. Chisholm, "Small Scale Radar Structure of Alberta Hailstorms," Preprints 12th Radar Meteorology Conference, American Meteorological Society, Boston, 1966, pp. 339-341.

13. L. J. Battan, "Duration of Convective Radar Cloud Units," Bull. Am. Meteorol. Soc., Vol. 34, 1953, pp. 227-228.

14. R. J. Donaldson, "Radar Reflectivity Profiles in Thunderstorms," J. Appl. Meteorol., Vol. 18, 1961, pp. 292-305.

15. R. L. Inman and J. E. Arnold, "Thunderstorm Characteristics. Final Report," Texas A&M University, Contract AF 19(604)-6136, 1961, pp. 8-73.

16. M. D. Hudlow and W. D. Scherer, "Precipitation Analysis for BOMEX Period III," NOAA Technical Report EDS 13, 1975.

17. R. A. Schleusener and L. O. Grant, "Characteristics of Hailstorms in the Colorado State University Network, 1960-1961," Preprints 9th Radar Meteorology Conference, American Meteorological Society, Boston, 1961, pp. 140-145.

18. M. D. Hudlow, "Radar Echo Climatology East of Barbados Derived from Data Collected During BOMEX," Preprints 14th Radar Meteorology Conference, American Meteorological Society, Boston, 1971, pp. 433-437.

19. R. J. Donaldson, "Analysis of Severe Convection Storms Observed by Radar — II," J. Appl. Meteorol., Vol. 16, 1959, pp. 281-287.

20. E. I. Boyd and D. J. Musil, "Radar Climatology of Convective Storms in Western Nebraska," Preprints 14th Radar Meteorology Conference, American Meteorological Society, Boston, 1970, pp. 433-437.

21. R. H. Douglas and W. Hitschfeld, "Studies of Alberta Hailstorms, 1957," McGill University, Stormy Weather Research Group, Science Department Report MW-27, 1958.

22. H. R. Byers and R. R. Braham, The Thunderstorm — Report of the Thunderstorm Project, U.S. Government Printing Office, Washington, DC, 1949.

23. E. M. Salman and K. S. Zhupaklien, "Some Results of Radar Investigations of the Vertical Structure of Showers and Thunderstorms," Glavnaia Geofizicheskaia Observatorua, Trudy, No. 159, 1967, pp. 59-64, Translation AD 667403.

24. H. W. Hiser and R. R. Adt, "Precipitation Echo Heights in South Florida," Preprints 9th Radar Meteorology Conference, American Meteorological Society, Boston, 1961, pp. 90-95.

25. R. E. Newell, "Some Radar Observations of Tropospheric Cellular Convection," Preprints 8th Radar Meteorology Conference, American Meteorological Society, Boston, 1960, pp. 315-322.

26. A. S. Dennis and F. G. Fernald, "Frequency Distribution of Shower Sizes," J. Appl. Meteorol., Vol. 2, 1963, pp. 767-769.

27. J. R. Miller, A. S. Dennis, J. H. Hirsh, and D. E. Cain, "Statistics of Shower Echoes in Western North Dakota," Preprints 16th Radar Meteorology Conference, American Meteorological Society, Boston, 1975, pp. 391-396.

28. "Radiometeorological Data," CCIR Report 235-2, 1974, pp. 92-112.